

1 Structural complexities and tectonic barriers controlling recent 2 seismic activity in the Pollino area (Calabria-Lucania, Southern Italy) 3 - constraints from stress inversion and 3D fault model building.

4
5 Daniele Cirillo^{1-2*}, Cristina Totaro²⁻³, Giusy Lavecchia¹⁻², Barbara Orecchio²⁻³, Rita de Nardis^{1-2*},
6 Debora Presti²⁻³, Federica Ferrarini¹⁻², Simone Bello¹⁻² and Francesco Brozzetti¹⁻²

7
8 ¹ Università degli studi “G. d’Annunzio” Chieti-Pescara, DiSPUTer, via dei Vestini 31, 66100 Chieti, Italy.

9 ² CRUST Centro interUniversitario per l’analisi SismoTettonica tridimensionale, Italy.

10 ³ Università degli studi di Messina, Dipartimento di Scienze Matematiche e Informatiche, Scienze Fisiche e Scienze della Terra
11 -Viale F. Stagno D’Alcontres, 98166, Messina, Italy

12 *Correspondence to: Daniele Cirillo (daniele.cirillo@unich.it) and Rita de Nardis (rita.denardis@unich.it)

13 **Abstract.** We reconstruct the 3D Fault Model of the structures causative of the 2010-2014 Pollino seismic activity by
14 integrating structural-geological and high-resolution seismological data. We constrained the model at the surface with fault-
15 slip data and at depth, by using the distributions of selected high-quality relocated hypocenters. Relocations were performed
16 through the non-linear Bayloc algorithm, followed by the double-difference relative location method HypoDD applied to a 3D
17 P-wave velocity model. Geological and seismological data highlight an asymmetric active extensional fault system
18 characterized by an E to NNE-dipping low-angle detachment, with high-angle synthetic splays, and SW- to WSW-dipping,
19 high-angle antithetic faults.

20 Hypocenter clustering and the time-space evolution of the seismicity suggest that two sub-parallel WSW-dipping seismogenic
21 sources, the Rotonda-Campotenese and Morano-Piano di Ruggio faults, are responsible of the 2010-2014 activity. The area of
22 the seismogenic patches obtained projecting the hypocenters of the early aftershocks on the 3D fault planes, are consistent
23 with the observed magnitude of the strongest events ($M_w=5.2$, and $M_w=4.3$). Since earthquake-scaling relationships provide
24 maximum expected magnitudes of $M_w=6.4$ for the Rotonda-Campotenese and $M_w=6.2$ for the Morano-Piano di Ruggio faults,
25 we may suppose that, during the sequence, the two structures did not release entirely their seismic potential.

26 The reconstructed 3D fault model also points out the relationships between the activated fault system and the western segment
27 of the Pollino Fault. This latter was not involved in the recent seismic activity but could have acted as a barrier to the southern
28 propagation of the seismogenic faults, limiting their dimensions and the magnitude of the generated earthquakes.

29 1 Introduction

30 In recent years, the reconstruction of 3D Fault Models (hereinafter referred to as 3DFM) obtained by integrating surface and
31 subsurface data, has become an increasingly practiced methodology for seismotectonic studies (*e.g.*, [Lavecchia et al., 2017](#);
32 [Castaldo et al., 2018](#); [Klin et al., 2019](#); [Ross et al., 2020](#); [Porreca et al., 2020](#); [Barchi et al., 2021](#); [Di Bucci et al., 2021](#); [SCEC,](#)
33 [2021](#)). Detailed structural-geological data are used to define the active faults geometry at the surface whereas high-quality
34 geophysical data are needed to constrain the shape of the sources at depth. The 3DFM building helps determining the spatial
35 relationships and the interactions between adjacent sources and identifying any barriers hampering at depth the propagation of
36 the coseismic rupture. Moreover, such an approach leads to accurately estimating the area of the seismogenic fault, and
37 therefore the expected magnitude.

38

39 In Italy, reconstruction of 3DFM could give important achievements in the Apennine active extensional belt which is affected
40 by significant seismic activity ([ISIDe, 2007](#); [Rovida et al., 2020](#)). This belt consists of ~NW-SE striking Quaternary normal
41 fault systems, and the related basins, located just west or within the culmination zone of the chain ([Calamita et al., 1992](#);
42 [Brozzetti and Lavecchia, 1994](#); [Lavecchia et al., 1994, 2021](#); [Barchi et al., 1998](#); [Cinque et al., 2000](#); [Brozzetti, 2011](#); [Ferrarini](#)
43 [et al., 2015, 2021](#)). Its structural setting is very complicated due to a polyphase tectonic history characterized by the
44 superposition of Quaternary post-orogenic extension on Miocene-Early Pliocene folds and thrusts and on Jurassic-Cretaceous
45 sin-sedimentary faults (*e.g.*, [Elter et al., 1975](#); [Ghisetti and Vezzani, 1982, 1983](#); [Lipmann-Provansal, 1987](#); [Mostardini and](#)
46 [Merlini, 1986](#); [Patacca and Scandone, 2007](#); [Vezzani et al., 2010](#); [Ferrarini et al., 2017](#); [Brozzetti et al 2021](#)).

47

48 Over time, detailed structural geological studies made it possible to recognize several seismogenic faults in the Apennine
49 active extensional belt ([Barchi et al., 1999](#); [Galadini and Galli, 2000](#); [Maschio et al., 2005](#); [Brozzetti, 2011](#)) and, in some cases,
50 to document, through paleo-seismological data, their reactivation during the Holocene ([Galli et al., 2020](#)). Furthermore, the
51 increasing availability of high-resolution imagery allows fault mapping at the sub-meter scale (*e.g.*, [Westoby et al., 2012](#);
52 [Johnson et al., 2014](#); [Cirillo, 2020](#); [Bello et al., 2021b, 2021c](#)), while accurate geophysical prospections (*e.g.*, Ground
53 Penetrating Radar), allows investigating the fault surface at shallow depths (few meters or tens of meters; *e.g.*, [Gafarov et al.,](#)
54 [2018](#); [Ercoli et al., 2013, 2021](#)). Conversely, the geometries of the faults at depth are rarely available since high-resolution
55 deep geological and geophysical constraints are often lacking (*i.e.*, deep wells and/or seismic profiles). In fact, in the last
56 decades, seismic reflection prospecting and deep-well exploitation for hydrocarbon research, avoided the area affected by
57 active extension, and focused on the eastern front of the chain and on the Adriatic-Bradanic foreland basin system
58 ([ViDEPI:www.videpi.com](#), last access: 19 April 2021).

59 This lack can be compensated with well relocated high-resolution seismological datasets, to be integrated with geological ones.
60 In Italy, datasets of highly precise re-located hypocenters were collected during recent seismic sequences ([Chiaraluce et al.,](#)
61 [2004, 2005, 2011, 2017](#); [Totaro et al., 2013, 2015](#)). These sequences include thousands of earthquakes (in confined volumes

62 of rock) which appear to roughly connect with the fault traces at the surface. Therefore, such distributions of earthquakes are
 63 generally referred to as ongoing rupture processes affecting an entire, or wide portions of, seismogenic faults.
 64 In some cases, very high-resolution hypocenter locations ([Chiaraluce et al., 2017](#); [Valoroso et al., 2017](#)), as well as reflection
 65 seismic lines, allow to clearly highlight the seismogenic structures at depth ([Sato et al., 1998](#); [Bonini et al., 2014](#); [Lavecchia](#)
 66 [et al., 2011, 2012a, 2012b, 2015, 2016](#); [Gracia et al., 2019](#); [Porreca et al., 2018](#); [Barchi et al., 2021](#)).
 67 The study area of this work includes the northern sector of the so-called “Pollino seismic gap” ([Fig. 1](#)), in which paleo-
 68 earthquakes up to $M=7$ are documented ([Michetti et al., 1997](#); [Cinti et al., 1997, 2002](#)), whereas the location and size of
 69 seismogenic sources are a matter of debate ([Michetti et al., 2000](#); [Cinti et al., 2002](#); [Papanikolaou and Roberts, 2007](#); [Brozzetti](#)
 70 [et al., 2009, 2017a](#)). [Brozzetti et al. \(2017a\)](#) mapped a set of active faults in the sector between the Mercure, Campotenese, and
 71 Morano Calabro Quaternary basins ([Fig. 1a](#)). During the 2010-2014, this area was affected by a low to moderate instrumental
 72 seismicity (Pollino seismic activity), climaxing with the 25 October 2012, M_w 5.2 Mormanno earthquake, and characterized
 73 by thousands of recorded events ([Totaro et al., 2013, 2015](#)). During the sequence, two others moderate events occurred close
 74 to the village of Morano Calabro: on 28 May 2012 (M_w 4.3), and on 6 June 2014 (M_w 4.0; [Fig. 1b](#)). According to [Brozzetti et](#)
 75 [al. \(2017a\)](#), the whole seismicity was arranged in two major clusters and a minor one. Each major cluster was associated with
 76 one moderate event and was generated by an independent seismogenic structure. The pre-existence of a seismic network, that
 77 was implemented after the beginning of the sequence, provided a high-quality database of relocated hypocenters ([Totaro et al.,](#)
 78 [2013, 2015](#); [Brozzetti et al., 2017a](#)).
 79
 80 In such context we reconstruct the 3DFM involved by the 2010-2014 seismic activity to investigate, at depth, the cross-cut
 81 relationships between the faults having different attitudes and timing of activation. Furthermore, we provide the geometric
 82 parameters of the sources to estimate the expected magnitudes. Finally, we discuss some 3D-seismotectonics methodological
 83 aspects which dwell on the improvements that the proposed procedure provides to the definition of the source model and on
 84 its limits.

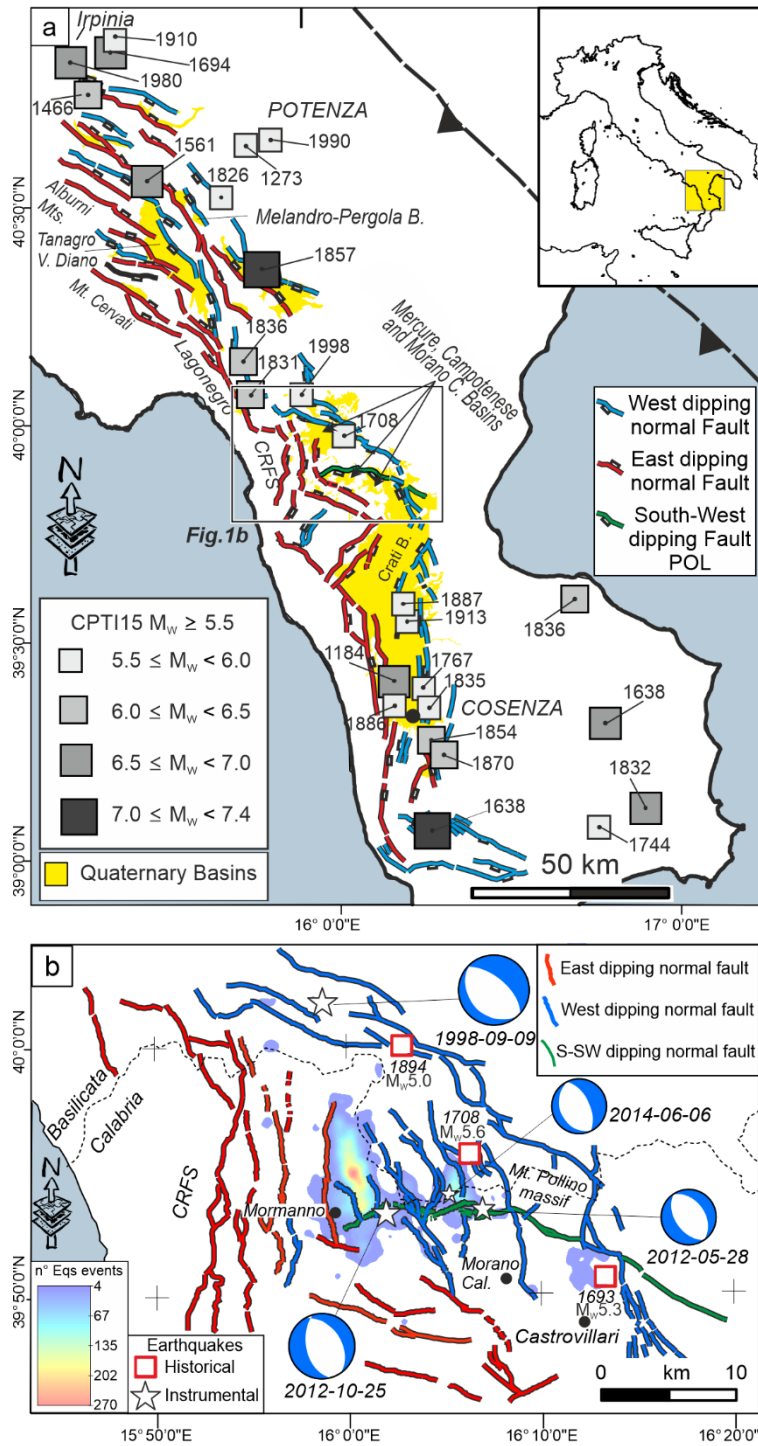


Figure 1: Seismotectonic context of the study area. (a) Active faults of the Southern Apennines with major historical and instrumental earthquakes from Parametric Catalogue of Italian Earthquakes, CPTI15 v3.0 (Rovida et al., 2020, 2021). (b) Normal faults cropping out between the Mercure, Campotenese, Morano Calabro, and Castrovillari Quaternary basins (after

89 Brozzetti et al., 2017a) with distribution of the 2010-2014 Pollino seismic activity (contoured areas) and focal mechanisms of
90 the events with $M_w > 4.0$ (Totaro et al., 2015, 2016).

91

92

93 2. Geological Setting

94

95 The Mt. Pollino massif is located at the Calabrian-Lucanian boundary (Fig. 1) in a sector of the Apennines structured during
96 the Middle-Late Miocene contractional tectonics which affected the western Adria Plate (D'Argenio, 1992; Patacca and
97 Scandone, 2007; Ietto and Barilaro, 1993; Iannace et al. 2004, 2005, 2007). The surface geology in this area is characterized
98 by the superposition of two main tectonic units derived from different paleogeographic domains. These are represented (from
99 bottom to top), by 1) the "Apenninic" units (or "Panormide"; Triassic - Early Miocene), which are characterized by carbonate
100 platform, including the Verbicaro and Pollino Units, locally intruded by basaltic rocks (Ogniben, 1969, 1973; Amodio Morelli
101 et al., 1976; Iannace et al., 2007; Patacca and Scandone, 2007; Vezzani et al., 2010; Tangari et al., 2018), 2) by the "Ligurian"
102 units (Late Jurassic – Early Cretaceous), that consist of ophiolites and deep-sea sedimentary deposits derived from the Western
103 Tethys oceanic basin (Ogniben, 1969, 1973; Amodio Morelli et al., 1976; Liberi et al., 2006; Liberi and Piluso, 2009; Filice
104 et al., 2015).

105

106 During uppermost Miocene and Pliocene times, the folds and thrusts pile was displaced by WNW-ESE-striking left-lateral
107 wrench faults (Grandjacquet, 1962; Ghisetti and Vezzani, 1982; Van Dijk et al., 2000). Subsequently, regional-scale
108 extensional fault systems, consisting of E- and W-dipping conjugate normal faults, dissected the Tyrrhenian side and the core
109 of the orogen which assumed a typical basin and range relief. This Quaternary phase caused the reactivation of the previous
110 strike-slip structures such as the Pollino fault (POL), whose normal to normal-oblique kinematics, has been documented since
111 the Early-Middle Pleistocene (Ghisetti and Vezzani, 1982, 1983, Brozzetti et al., 2017a).

112

113 At present, the age of onset of the extensional tectonic is still under discussion; it is referred by some authors to the Early
114 Pleistocene (Ghisetti and Vezzani, 1982; Schiattarella et al., 1994; Papanikolaou and Roberts 2007; Barchi et al., 2007; Mattei
115 et al., 2007; Cifelli et al., 2007; Amicucci et al., 2008; Brozzetti, 2011; Robustelli et al., 2014), while it would not be older
116 than the Middle Pleistocene, according to others (Caiazza et al., 1992; Cinque et al. 1993; Hyppolite et al., 1995; Cello et al.,
117 2003; Giano et al., 2003; Spina et al., 2009; Filice and Seeber, 2019).

118

119 In the Campania-Lucania and north-Calabria sectors of the southern Apennines, the active extensional belt includes three main
120 alignments of normal faults and Quaternary basins, arranged in a right-lateral en-echelon setting (Fig. 1a). From north to south
121 they are: the internal alignment, including the Irpinia fault, the Melandro-Pergola and Agri basins the intermediate one,
122 developing from the Tanagro-Vallo di Diano basins to the Mercure-Campotenese and Morano Calabro basins the external

alignment, developing from the Castrovillari fault to the southern Crati basin (Pantosti and Valensise, 1990, 1993; Ascione et al., 2013; Galli and Peronace, 2014; Ghisetti and Vezzani, 1982, 1983; Barchi et al., 1999, 2007; Blumetti et al., 2002; Amicucci et al., 2008; Maschio et al., 2005; Villani and Pierdominici, 2010; Brozzetti, 2011, Faure Walker et al., 2012; Brozzetti et al., 2009, 2012, 2017a, 2017b; Robustelli et al., 2014; Sgambato et al., 2020; Bello et al., 2021a).

All along the above alignments, the geometry and kinematics of the major normal faults are kinematically compatible with a SW-NE direction of extension (Maschio et al. 2005; Brozzetti, 2011; Brozzetti et al., 2009; 2017a). A similar orientation of the T-Axis is obtained from the focal mechanisms of the major earthquakes from CMT and TDMT databases (Pondrelli et al., 2006; Scognamiglio et al., 2006; Montone and Mariucci., 2016; Totaro et al., 2016) and from GPS data (D'Agostino et al., 2014), Cheloni et al. (2017). The recent activity of these normal fault systems is firstly suggested by the control exerted on the distribution of seismicity, as shown by the location of upper crustal instrumental earthquakes (ISIDe Working Group, 2007; Brozzetti et al., 2009; Totaro et al., 2014, 2015; Cheloni et al., 2017; Napolitano et al., 2020, 2021; Pastori et al., 2021; Sketsiou et al., 2021; De Matteis et al., 2021) and of destructive historical events (Fig. 1; Rovida et al., 2021).

The area affected by the 2010-2014 seismicity extends from the Mercure to the Campotenese and Morano Calabro basins, along the intermediate extensional fault alignment which, according to previous literature, consists of three main sets of genetically-linked normal and normal-oblique active faults (Brozzetti et al., 2017a; Figs 1b, 2; Acronyms list in Supplementary Text 1). The first one, referred to as the Coastal Range Fault Set (CRFS; red lines in Figs 1b, 2) dips E- to NNE and encompasses four sub-parallel major fault segments named, from west to east, Gada-Ciagola (GCG), Papasidero (PPS), Avena (AVN) and Battendiero (BAT). Their strike varies southward from N-S to WNW-ESE.

The other two fault sets strike ~NW-SE and dip ~SW (blue lines in Figs 1b, 2). The western one, developing from Rotonda to Campotenese villages, consists of two main right-stepping en-echelon segments. They are referred to as ROCS system and include the Rotonda-Sambucoso (RSB) and Fosso della Valle-Campotenese (VCT; Fig. 2). The eastern set, including the en-echelon Castello Seluci - Piana Perretti - Timpa della Manca (CSPT), the Viggianello-Piani del Pollino (VPP) and the Castrovillari (CAS) faults, represents the break-away zone of the Quaternary extensional belt. In the area between these two W-dipping sets, the W to NW-dipping Morano Calabro-Piano di Ruggio (MPR) and Gaudolino (GDN) faults, show evidence of Late Quaternary activity (Brozzetti et al., 2017a; Fig. 2).

GPS and DInSAR analysis demonstrated as the Pollino area was affected by important deformation rates during the 2010-2014 seismic activity, with increasing and decreasing of slip values due to the temporal and spatial variation of the recorded seismicity (Passarelli et al. 2015).

151

152

153 **3 Seismotectonic Setting**

154

According to Michetti et al. (1997, 2000) and Cinti et al. (1997, 2002), POL and the adjacent CAS faults were associated with at least two strong earthquakes, (M 6.5 and M 7.0), occurred in the period 2000-410 B.C. and 500-900 A.D., respectively. The

epicenter of the 8 January 1693 earthquake (M 5.3, CPTI15, [Rovida et al., 2020, 2021](#); [Fig. 1b](#), [Fig. 2](#)) is also located within the hanging wall of the CAS and at the footwall of the MPR fault, some kilometers eastward of the 2012 and 2014 Morano Calabro strongest events. The epicenter locations of the M_w 5.5, 1708, and M_w 5.1, 1894 earthquakes ([Rovida et al., 2021](#)), close to the northern termination of the RSB and within its hanging wall, allows hypothesizing the latter fault as the possible seismogenic source.

The main instrumental event recorded in the Pollino area is the M_w 5.6 Mercure earthquake (9 September 1998; [Fig. 1b](#)), which was followed by some hundred aftershocks and that was associated by [Brozzetti et al. \(2009\)](#) with the SW-dipping CSPT ([Fig. 1b](#), [Fig. 2](#)), located some kilometers to the NE of the Mercure basin.

The focal mechanisms of the three strongest earthquakes (M_w 5.2, 25 October 2012-Mormanno; M_w 4.3, 28 May 2012-Morano Calabro; M_w 4.0, 6 June 2014-Morano Calabro) are consistent with extensional (upper crustal) deformations ([Montone and Mariucci 2016](#); [Mariucci and Montone 2020](#)).

All the associated WSW-ENE oriented T-axes are also quite parallel to the geological and seismological least compressional axis, as provided by the tensorial analysis in the neighbouring Mercure area ([Brozzetti et al., 2009](#); [Ferranti et al., 2017](#)) or derived from borehole breakouts ([Montone and Mariucci 2016](#); [Mariucci and Montone 2020](#)), and GPS data ([D'Agostino et al., 2014](#)). As discussed by [Totaro et al. \(2015, 2016\)](#) and [Brozzetti et al. \(2017a\)](#), the available focal solutions well correlate with the Quaternary normal faults recognized in the epicentral area, represented by N-S to NNW-SSE-striking (W-dipping) seismogenic sources.

Correlating the hypocenters distribution with the active faults at surface, the seismogenic source of the 25 October 2012 Mormanno Earthquake (M_w 5.2), is identifiable in both the segments of the WSW-dipping ROCS system (RSB and VCT in [Fig. 1b](#), [Fig. 2](#)). These faults dip 70° - 75° , at the surface, and would reach a dip of $\sim 55^\circ$ at depth ([Brozzetti et al., 2017a](#)).

Through similar reasonings, the WSW-dipping MPR fault was suggested to be the causative fault of the eastern Morano Calabro cluster ([Fig. 1b](#)) and of its two major events (M_w 4.3, 28 May 2012 and M_w 4.0, 6 June 2014). The fault extends for ~ 7 km in a N170 direction and is co-axial with the W-dipping nodal planes of the two main events of the sequence ([Fig. 1b](#)).

The partial reactivation of the CAS could be invoked to explain the minor cluster of seismicity recorded at the eastern side of the study area, although some of the events seem to be located at its footwall.

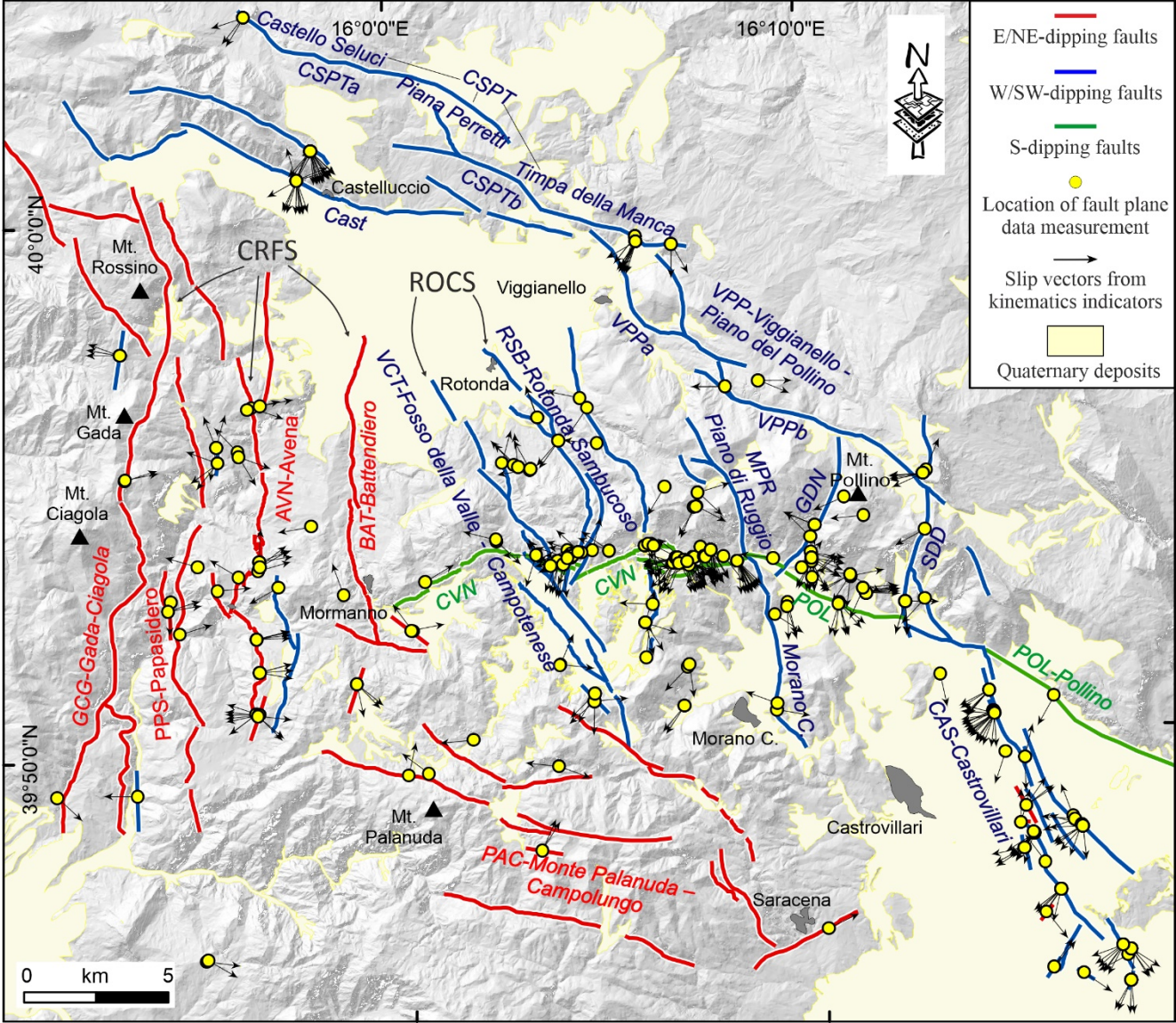
4 Data and Methods

4.1 Structural survey and fault kinematic analysis

We performed a series of fieldwork campaigns, at 1:25.000 scale, in the study area and surrounding sectors, to collect fault-slip data to be integrated with the geological-structural observations reported in [Brozzetti et al. \(2017a\)](#). We used the Fieldmove App (PetEx Ltd., version 2019.1) installed on a tablet computer to acquire the data in the field, and we managed them in ArcGIS v.10.8 (ArcMap©). [Fig. 2](#) shows the location of the survey sites, considered structurally homogeneous outcrops falling

190 within a maximum distance of 500 m (see also [Supplementary Fig. 2](#)). The overall fault-slip dataset was first subdivided in
 191 minor and local homogenous kinematic subsets, the latter represented as pseudo-focal mechanisms using FaultKin 8 software
 192 ([Marrett and Allmendinger, 1990](#); [Allmendinger et al., 2012](#); [Fig 3](#)). The fault/slip data were subsequently inverted (see
 193 following sec. 4.3).

194
 195



196

197 **Figure 2:** Structural Map at the Calabrian-Lucanian boundary (after [Brozzetti et al., 2017a](#)) with location of fault-slip data
 198 measurements. Fault key: CRFS= Coastal Range Fault Set; GCG= Gada-Ciagola fault; PPS= Papasidero fault; AVN= Avena
 199 fault; BAT= Battendiero fault; ROCS= Rotonda-Campotenese fault system; VCT= Fosso della Valle-Campotenese fault;

200 RSB= Rotonda-Sambucoso; CVN= Cozzo Vardo-Cozzo Nisco fault; MPR= Morano Calabro-Piano di Ruggio fault; VPP=
201 Viggianello - Piani del Pollino fault set; VPPa= Viggianello-Prastio fault; VPPb= Vacquarro-Piani del Pollino fault; GDN=
202 Gaudolino fault; POL= Pollino fault; CAS= Castrovillari fault; SDD= Serra Dolcedorme fault; PAC= Monte Palanuda –
203 Campolungo fault; Cast= Castelluccio fault; CSPT= Castello Seluci-Piana Perretti-Timpa della Manca fault; CSPTa= Castello
204 Seluci - Piana Perretti fault; CSPTb= Timpa della Manca - La Fagosa fault.
205
206

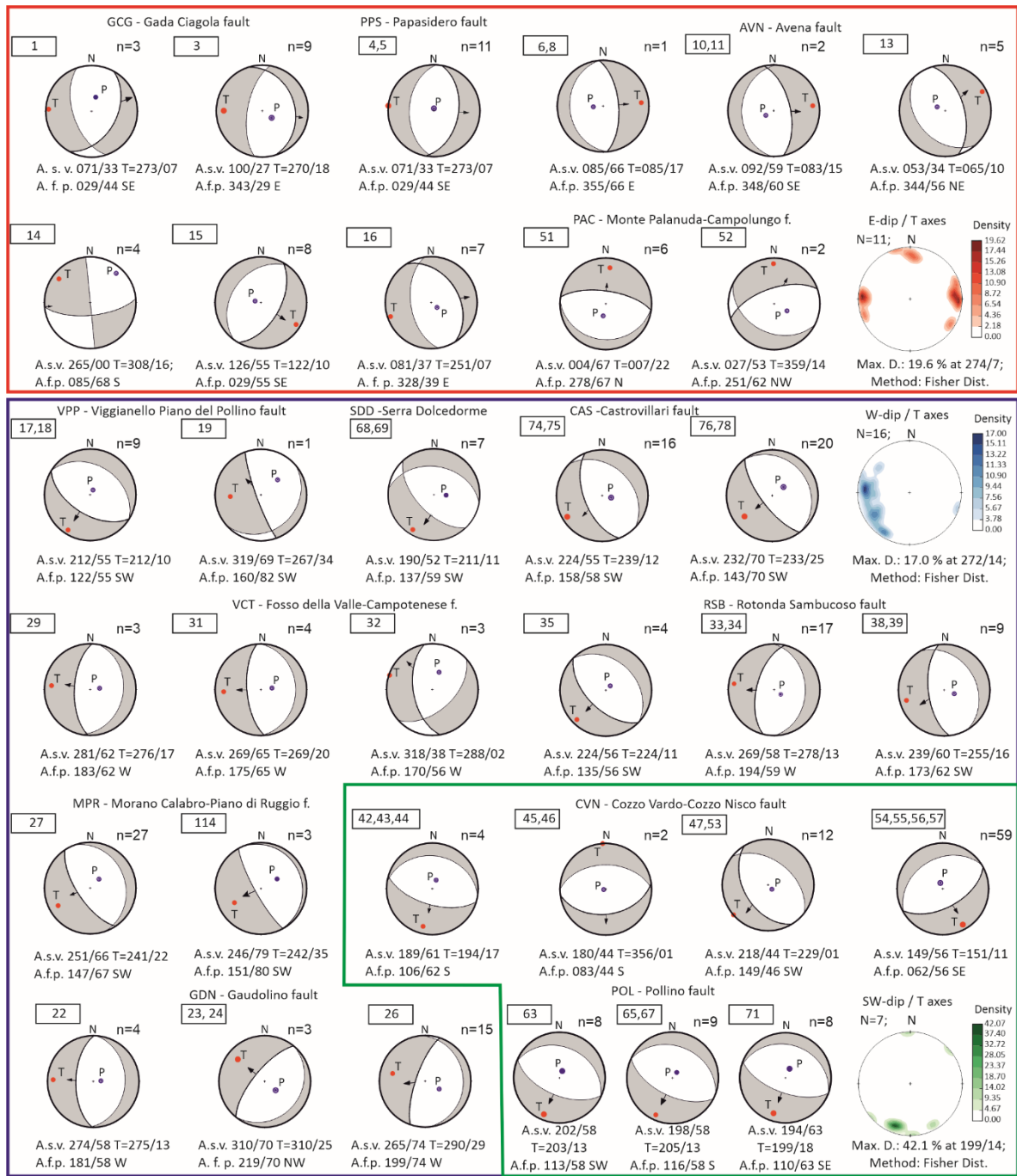


Figure 3: Kinematic analysis and pseudo-focal mechanisms obtained from fault/slip data using the FaultKin 8 software (Allmendinger et al., 2012). Pseudo-focal mechanisms are boxed with different colors on the basis of the fault system to which they belong to (color key as in the map of Fig. 1, Fig. 2). For each fault system, the density contour of the T-axis computed for each focal mechanism is reported (lower hemisphere projection). A.s.v.=Average striae value, A.f.p.=Average fault plane,

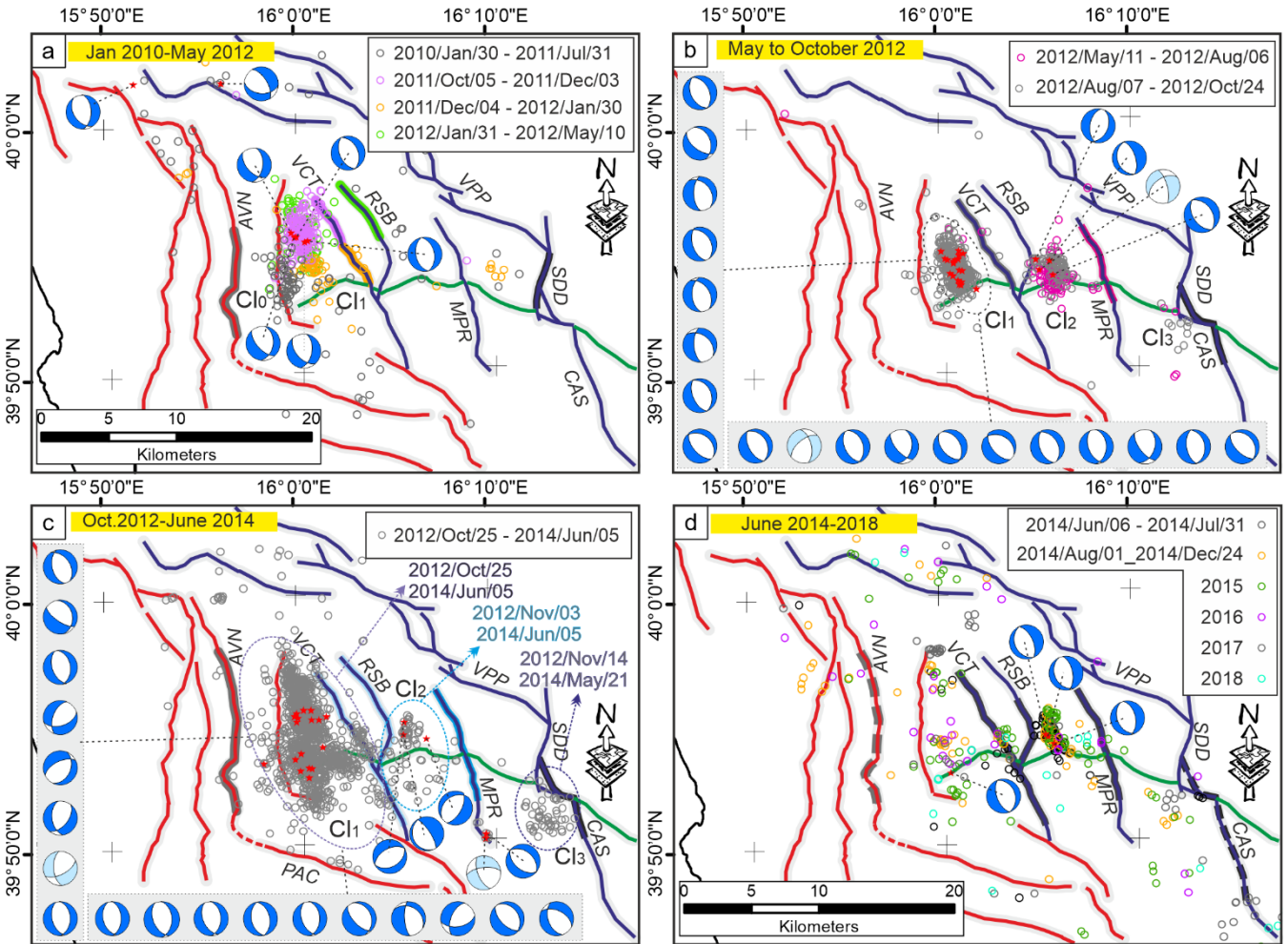
213 n=number of fault-plane measurements. Numbers in the rectangles (top left of each focal mechanism) refer to the group of
214 fault/slip data belonging to or neighbouring of a single site (location in [Supplementary Fig. 2](#)).

215

216 4.2 Hypocenter location

217

218 To better characterize the 3D features of the tectonic structures located in the study area, we performed a high-quality
219 hypocenter location. We enlarged, with respect to previous works by [Totaro et al. \(2013, 2015\)](#) and [Brozzetti et al. \(2017a\)](#),
220 the time window for earthquake analyses, (i.e., January 2010 and October 2018) selecting earthquakes with local magnitude
221 greater than 1.0 and hypocentral depth range 0-30 km from the INGV and the University of Calabria database (www.ingv.it,
222 last access: 19 April 2021; <http://www.sismocal.org>, last access: 19 April 2021). Automatic and manually revised P- and S-
223 wave arrival time picks have been selected for this dataset. The recording network, including both temporary and permanent
224 stations managed by the University of Calabria and INGV ([D'Alessandro et al., 2013](#); [Margheriti et al., 2013](#)), consisted of 61
225 stations with a maximum epicentral distance of 150 km ([Supplementary Fig. 1](#)). We computed accurate absolute hypocenter
226 locations by applying first the non-linear Bayloc earthquake location algorithm ([Presti et al., 2004, 2008](#)) and subsequently the
227 double-difference relative location method HypoDD (v.2; [Waldhauser, 2001](#)), and using the 3D velocity model by [Orecchio](#)
228 [et al. \(2011\)](#). The Bayloc algorithm gives for each earthquake a probability density cloud with shape and size related to the
229 main factors involved in the location process (e.g., network geometry, picking errors), and allows a generally more accurate
230 estimate of hypocenter parameters and location uncertainties with respect to the more commonly used linearized location
231 methods (e.g., [Lomax et al., 2000](#); [Husen and Smith, 2004](#); [Presti et al., 2008](#)). The application of the Bayloc algorithm provide,
232 on average, horizontal and vertical errors of the order of 1.0 and 1.5 km, respectively, allowing us to obtain a well-constrained
233 database. As the second step, we apply the HypoDD algorithm, which minimizes phase delay-time residuals between pairs of
234 events recorded at common stations ([Waldhauser and Ellsworth, 2000](#)). We compute the delay times from each event to its 30
235 nearest neighbors within 10 km distance, and to further ensure the robustness of the double-difference inversion only event
236 pairs with at least eight phases observed at common stations were used. The final relocated dataset consists of 3109 events
237 ([Fig. 4](#) and [Supplementary Fig. 1](#)). During the decade before the 2010-2014 Pollino sequence, the instrumental data available
238 within a range of nearly 75 km from the Mercure basin, referred to background seismic activity ([Frepoli et al., 2005](#); [Castello](#)
239 [et al., 2006](#); [Brozzetti et al., 2009](#)). A significant seismic activity which affected the region, was the moderate magnitude 1998-
240 1999 Mercure sequence that developed in the northern part of the homonym Quaternary basin ([Supplementary Fig. 1](#); [Guerra](#)
241 [et al., 2005](#); [Arrigo et al., 2005](#); [Brozzetti et al., 2009](#)) and showed some similarities to the recent Mercure-Pollino sequence
242 (e.g., prevalent kinematics of focal mechanisms and hypocentral depth range). We explored the data available for this seismic
243 activity, to compute a high-quality earthquake location, following the procedure described above for the 2010-2018
244 earthquakes dataset. Since the recording network operating during the 1998-1999 seismic phase was significantly different
245 from today, in terms of number of stations deployed in the region and their spatial distribution, the available data do not allow
246 to reach the high level of constrain needed to perform the 3D structural model reconstruction.



248

249 **Figure 4:** Time-space evolution of the 2010-2018 seismic activity in the Pollino area. Each panel shows the distribution of
250 focal mechanisms (Totaro et al., 2015, 2016) and epicenters concentrated in a series of neighbouring clusters numbered as Cl
251 0, 1, 2, and 3 from west to east, according to their activation time. See section 5.2 for the sequence description. The Focal
252 mechanisms are classified following Frohlich (2001) kinematics classification (blue beachball= Normal kinematics; light
253 blue= Normal Strike kinematics). Red small circles represent the epicentres of focal mechanism solutions.

254

255 **4.3 Geological and seismological stress tensor inversion**

256

257 To investigate the coherence between the geological and the seismological stress fields, we applied stress tensor inversions to
258 the available fault-slip data (Figs. 2, 3) and focal mechanisms (Fig. 4). We used the ‘TENSOR’ program and the inversion
259 procedure proposed in Delvaux and Sperner (2003). We applied it, separately, on the different datasets. The procedure
260 computes the orientation of the three principal axes of the stress ellipsoid (σ_1 , σ_2 , σ_3) and the stress ratio $\Phi = (\sigma_2 - \sigma_3) / (\sigma_1 - \sigma_3)$

261 that optimize the misfit Function (*i.e.*, F5 in 'TENSOR' program, described as f_3 in [Delvaux and Sperner, 2003](#)). The latter is
 262 built i) to minimize the slip deviation between the observed slip line and resolved shear stress (30° misfit value is not expected
 263 to be exceeded), and ii) to favor higher shear stress magnitudes and lower normal stress to promote slip on the plane. The
 264 inversion procedure provides for the preliminary (kinematic) analysis of data using an improved version of the Right Dihedron
 265 method ([Angelier and Mechler, 1977](#)) to determine the starting model parameters (*e.g.*, the reduced stress tensor). The stress
 266 ellipsoid is then computed through a 4D grid-search inversion involving several runs during which the reduced tensor is rotated
 267 around each stress axis with a decreasing range of variability (from $\pm 45^\circ$ to $\pm 5^\circ$), and the full range of Φ values (0-1) is
 268 checked. Each step attempts to find the parameters that minimize the misfit function and that are used as a starting point for
 269 the next run (see for details [Delvaux and Sperner, 2003](#)).
 270 The geological data input consists of 268 quality selected fault/slip data measured in the study area ([Fig. 2, 3](#)). During the
 271 formal inversion, the same weight value was assigned to each fault. The seismological data input is represented (initially) by
 272 both nodal planes of each focal mechanism; afterward, the plane that is best explained by the stress tensor in terms of the
 273 smallest misfit function is considered as the actual fault plane ([Delvaux and Barth, 2010](#)). The inverted seismological data are
 274 represented by focal mechanisms from [Totaro et al. \(2015, 2016\)](#) and reported in [Fig. 4](#). An exponential weighting factor
 275 (corresponding to the earthquake magnitudes) has been assigned to account for the prevailing kinematics of the most energetic
 276 events. The final inversion ([Fig. 5](#)) includes only the fault- and focal-planes that are best fitted by a uniform stress field ([Gephart
 277 and Forsyth, 1984](#)).

278

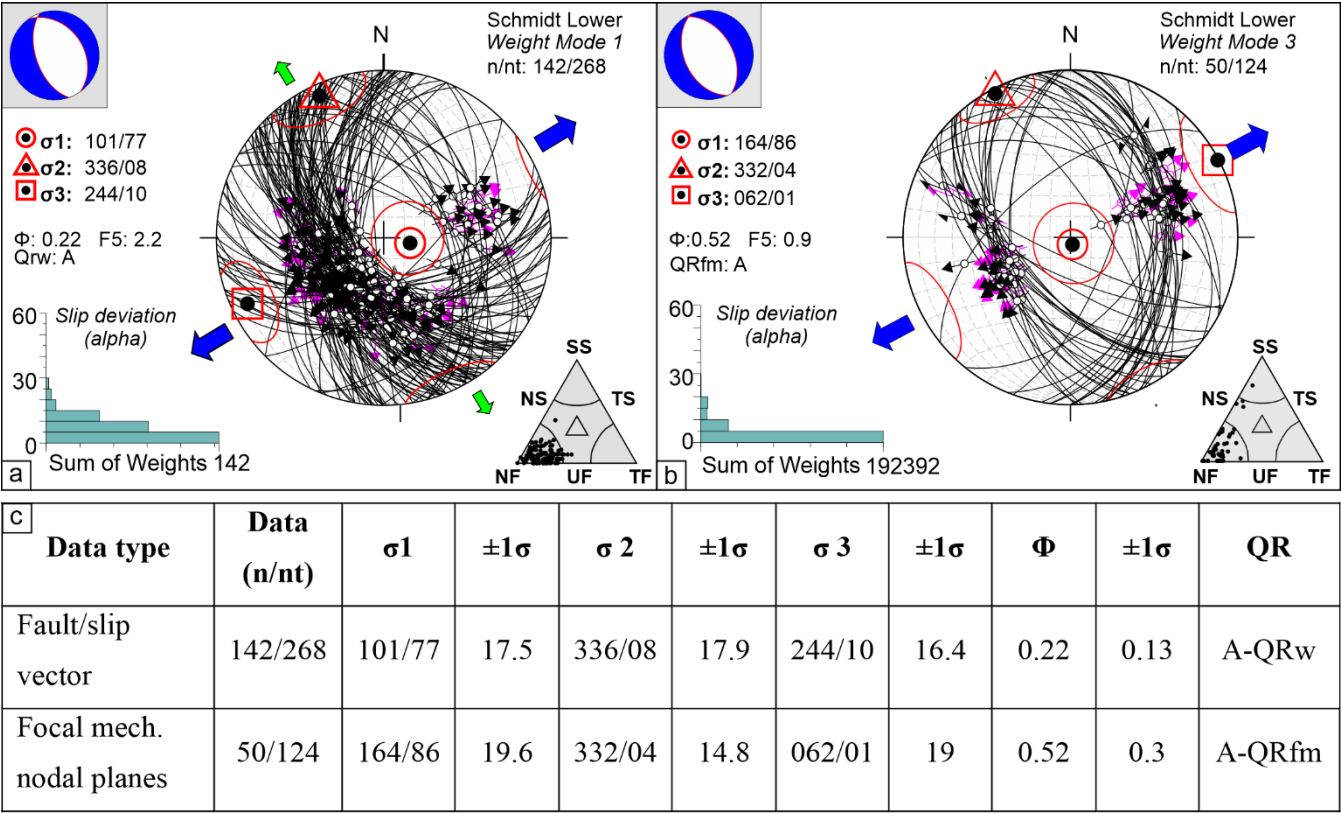


Figure 5: Stress inversion results for the geological- (a) and seismological (b) data. On the lower hemisphere Schmidt nets, the pairs fault plane/slickensline pairs (a) and focal plane/kinematic indicators (rake) (b) are reported (great circles represent the fault planes; the dark and pink arrows indicate the measured slip directions (or rake) and resolved shear stress respectively). The histograms represent the corresponding misfit angles vs. the number of data points; nt = total number of fault data; n = number of successfully inverted fault data; σ_1 , σ_2 , σ_3 = principal stress axes; Φ = stress ratio = $(\sigma_2 - \sigma_3) / (\sigma_1 - \sigma_3)$; the quality ranking factors (QR) and the stress inversion parameters with associated uncertainties (1σ standard deviations) are listed in panel (c). On the small upper left nets, the computed stress field represented as a focal mechanism is also reported. The triangles reported on the lower right corner of each panel (a) and (b) show the kinematic classification of data according to [Frohlich \(2001\)](#). (c) Geological and seismological stress tensor parameters computed starting from slip-vector measurements collected along the investigated fault systems ([Figs. 2, 3](#)) and focal mechanisms, respectively (see. Sect. 3 and [Fig. 4](#)). Key: nt = total number of data (e.g., plane/slickensline); n = inverted data; σ_1 , σ_2 , σ_3 = principal stress axes; Φ = stress ratio = $(\sigma_2 - \sigma_3) / (\sigma_1 - \sigma_3)$. QR = quality ranking: AQRw as in [Sperner et al. \(2003\)](#) and A-QRfm as in [Heidbach et al. \(2010\)](#).

4.4 3D Model building

Following the methodology defined by the Community Fault Model of Southern California ([Nicholson et al., 2014](#); [Nicholson](#)

et al., 2015; Plesch et al., 2014), also applied for recent Italian earthquakes (Lavecchia et al., 2017; Castaldo et al., 2018; Bello et al., 2021a), we obtained the 3DFM of the Pollino area by integrating Quaternary fault mapping (Brozzetti et al., 2009, 2017a; this paper) with high-quality seismicity dataset (2010-2018), and by using the Move suite software v. 2019.1 (Petroleum Experts Ltd).

302

In particular, we created several sets of closely spaced transects (distance=2 km) to cross and sample the seismogenic fault zones in different directions (Fig. 6). The first two sets (oriented SW-NE and NW-SE) are respectively ~perpendicular (e.g., sections a, b in Fig. 6) and ~sub-parallel (e.g., sections c-e in Fig. 6) to the ROCS (VCT and RSB), and MPR active faults (e.g., sections f in Fig. 6). A further NNE-SSW-striking set of transects was traced ~ perpendicular to the active fault alignment bounding eastward the study area, which includes the CSPT and VPP faults (sections g and h in Fig. 6).

The 3DFM building was carried out following three steps graphically depicted in Fig. 7 and synthetically described below.

309

310 *Step 1 - Extrusion of fault traces to shallow depth*

The traces of the Quaternary faults are “extruded” to a pre-set depth of 2 km b.s.l, according to the fault planes dip measured in the field. In the absence of measured dip-angles, we assumed a fixed value of 60° . The obtained so-called “fault ribbons” are rimmed upward by the topographic surface (a 10 m-resolution DEM; Tarquini et al., 2012).

314

315 *Step 2 - Down-dip extrapolation of the faults along seismological sections*

Starting from the analysis of the seismological transects (Fig. 6), we traced the deep geometries by connecting the fault ribbons with the seismicity clusters at depth (Fig. 7b,c) downward to the base of the seismogenic layer.

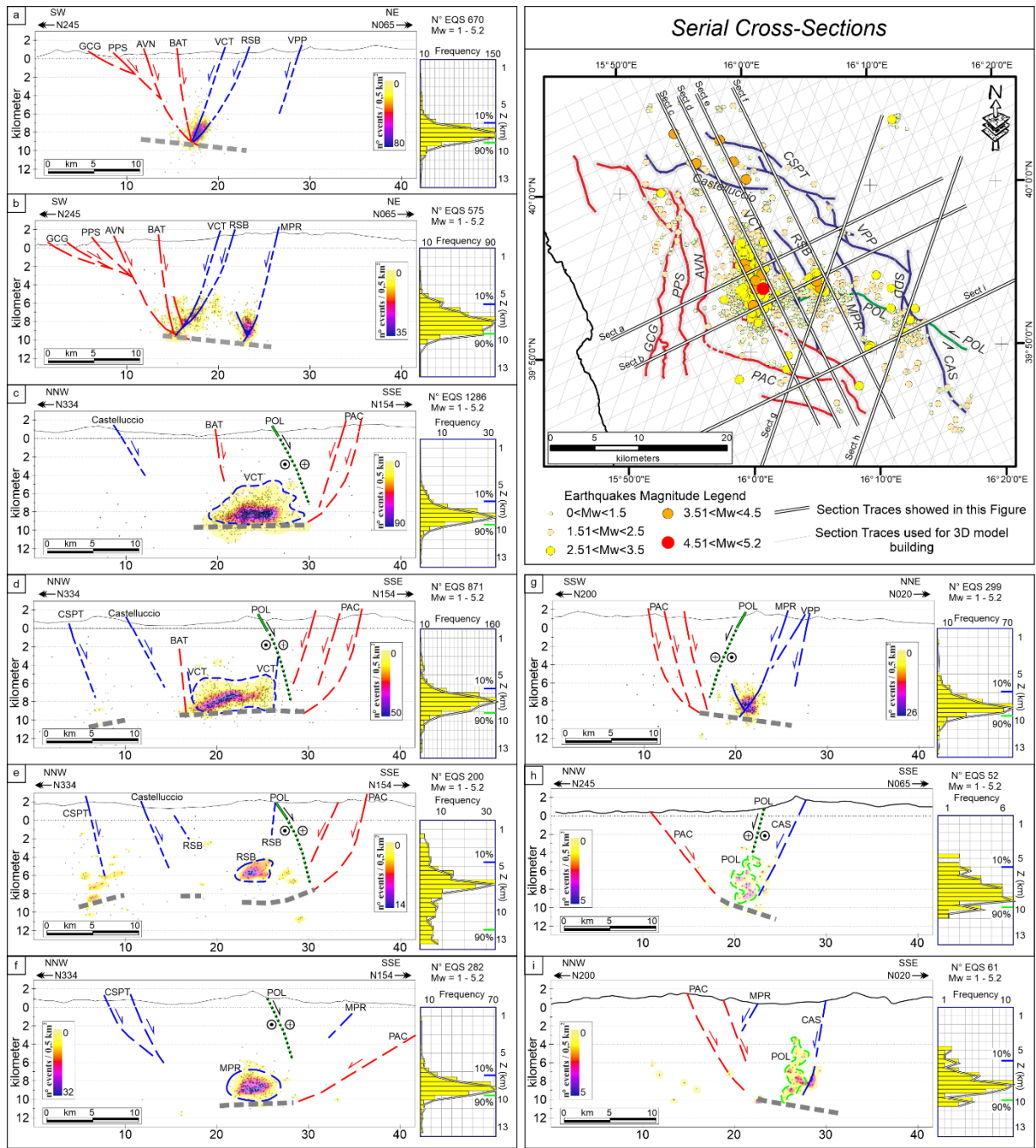
318

319 *Step3 - Building of 3D fault surfaces*

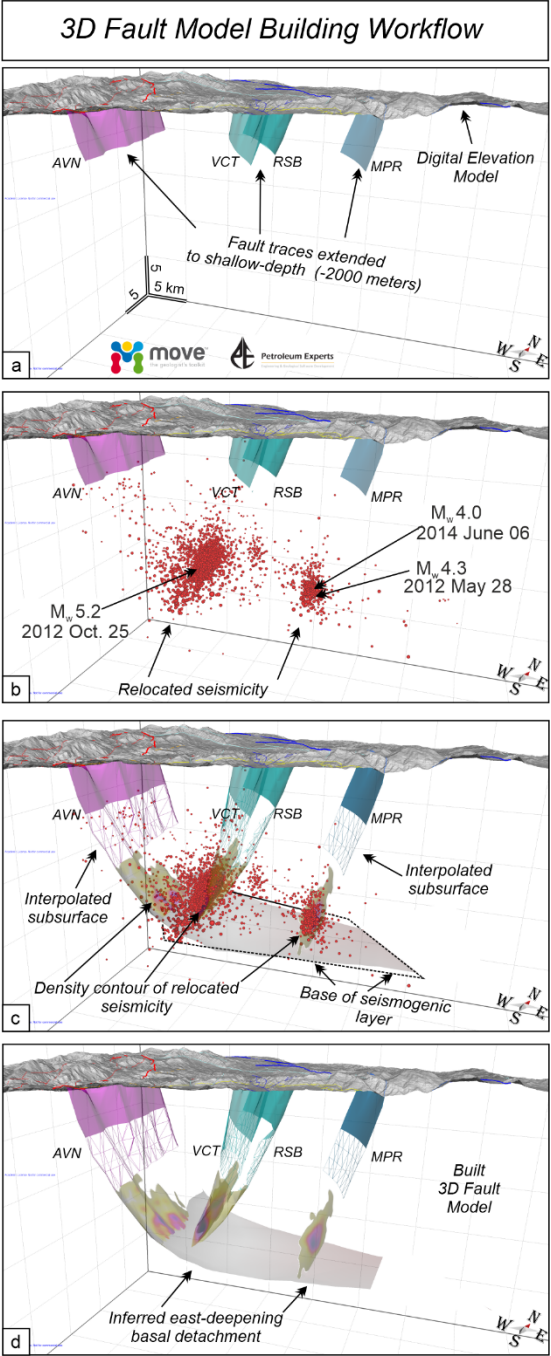
This step allows reaching the final 3D reconstruction (Fig. 7c,d) by interpolating, through the Delaunay triangulation method (Delaunay, 1934) all the fault lines as interpreted along the seismological cross-sections (Step 2). The result is the fault plane surface that best approximates and connects the clusters of seismicity and the surface geology (represented by the fault traces extruded).

324

325



326
 327 **Figure 6:** Epicentral map (upper-right panel) and hypocentral distributions (sections a-i) of the 2010-2018 seismic activity
 328 occurred in the Pollino area. In the cross-sections the earthquakes (grey dots) within a half-width of 1 km have been also
 329 reported also as density contours computed using Kernel Density Estimation. The histograms related to each section shows
 330 the depth distribution of the hypocenters. The traces of all the serial cross-sections analyzed in this study are reported in map
 331 view (upper-right panel) as thin grey lines, while the bold lines relate to the sections (a-j) shown in this figure.



333

334

335

336

337

Figure 7: 3D fault model building, from the surface (10 m-resolution DEM from Tarquini et al., 2012) to the base of the seismogenic layer. Faults acronyms as in Fig. 2. (a) “Fault ribbons” obtained by extruding the fault traces mapped at the surface down to 2 km depth, and considering the fault dip-angles measured in the field. (b) 3D fault model as in (a) with the relocated seismicity. (c) Fault extrapolation at (seismogenic) depth through the clusters of hypocenters; the modeled faults connect the

338 ribbons with the zones at the depth where concentrations of hypocenters are higher. The density contours of the seismicity and
339 the base of the seismogenic layer are also shown (see also panel d). (d) Final 3D fault model obtained integrating the detailed
340 Quaternary fault pattern with the high-quality 2010-2018 seismicity dataset.
341

342 **5 Results**

343 **5.1 Geological and Seismological Stress Tensors**

344

345 The computed geological stress tensor (Fig. 5) shows a relevant percentage of fault/slip vector pairs (~53%) consistent with a
346 uniform extensional stress field which is characterized by a N244 trending- and sub-horizontal σ_3 . The stress ratio
347 $\Phi=0.22\pm0.13$ and the rank quality is QRw=A (ranking as in Sperner et al., 2003). Nearly all the kinematic axes related to the
348 inverted data belong to a normal-fault regime as also pointed out by the triangle in Fig. 5 (Frohlich 2001).

349 The seismological stress tensor (Fig. 5b) obtained from inverting 50 actual fault planes (nt = 124 nodal planes), shows a normal
350 fault regime with an ENE-WSW trending and sub-horizontal σ_3 (N062/01 ± 19). The stress ratio $\Phi=0.52 \pm 0.3$ and the rank
351 quality is QRfm=A (ranking as in Heidbach et al., 2010). Most of the nodal planes show normal-fault kinematics (see Fig. 5b).
352 In both the inversions, a normal-fault regime with sub-horizontal and collinear (~SW-NE trending) σ_3 -axis has been obtained.
353 This result points out the coherence between the geological (long-term) and the present-day stress field and the persistence of
354 this extensional regime at least since the Middle Pleistocene (Brozzetti et al., 2017).

355 In addition, it is worth noticing as 76% of the successfully inverted fault/slip vector pairs are related to the active fault planes
356 belonging to the E- and W-dipping domains (Fig. 5a) while the remaining 24% include data related to the S-dipping system
357 (CVN and POL). The evidence together with the similarity between the computed stress tensors is consistent with the prevalent
358 activation, in the Late Quaternary, of the E- and W-dipping fault systems

359

360

361 **5.2 Time-space evolution of the Pollino sequence**

362

363 The 2010-2018 seismic activity in the Pollino-Mercure area followed a peculiar evolution over time (Fig. 4) with epicenters
364 concentrated in a series of neighboring clusters, numbered as Cluster 0, 1, 2, and 3, from west to east, according to their
365 activation time. Such clusters, independent and unconnected to each other are related to fault segments that are not in an along-
366 strike continuity.

367

368 Cluster 0 (30/01/2010 - 31/07/2011), includes low magnitude ($1.0 \leq M_L \leq 2.9$) activity located in an NNE-SSW oriented sector
369 at the western boundary of the epicentral area. It is delimited westward by the more external segment of the E-dipping CRFS.
370 Cluster 1 started after 05/10/2011 and lasted for the entire 2011-2014 seismic activity. It extended continuously, both
371 northward and southward, reaching a NW-SE length of ~12 km (Fig. 4a-c). It comprehends the higher number of earthquakes

and is largely the major cluster as regards the wideness ($\sim 60 \text{ km}^2$) and energy release. It includes 30 events with $M_L \geq 3.0$ besides the 25 October 2012 strongest event of the whole Pollino seismic activity. During the 2015-2018 interval, Cluster 1 area was affected by low seismic activity, mostly distributed in its northern and southern portions; conversely, its central part, where epicenters were particularly dense between 2011 and 2014, became less active. Overall, the surface extent of Cluster 1, which partly overlaps with Cluster 0, is limited eastward by the W-dipping RSB and VCT faults. Its southern boundary nearly coincides with the southeastern continuation of the AVN fault (PAC, Fig. 4c).

Cluster 2 started in May 2012 in the sector between the two WSW-dipping RSB and the MPR faults. It elongates in N-S direction, for $\sim 7 \text{ km}$ to the northwest of the Morano Calabro town. Afterward, it was nearly continuously active, particularly during the periods May 2012 - October 2014 (Fig. 4b,c); also in the period 2015-2018, significant seismicity persisted (Fig. 4d). Cluster 2 includes mainly low-magnitude events besides the strongest ones of 28 May 2012 and 6 June 2014 and three other earthquakes with $3.0 \leq M_L \leq 3.5$.

Further east, in the sector comprised between MPR and the alignment VPP-SDD-CAS faults, a minor cluster of seismicity (Cluster 3) develop since December 2011 (Fig. 4a). Since then (2011-2018) it was affected by poor and low-magnitude seismicity, which however was clearly above the threshold of background seismicity, with two $M_L=3.0$ events (Fig. 4a-d).

5.3 3D Fault Model of the Pollino area fault system

The obtained 3DFM (Fig. 8), which includes the seismogenic fault system involved during and after the 2010-2014 Pollino seismic activity, (CRFS, ROCS, and MPR) also encompasses those faults (GCG, PPS, AVN, BAT, CSPT, VPP, SDD, CAS) that, while showing no direct evidence of recent seismic activity, play a significant role in the seismotectonic frame of the area.

The westernmost fault structures (*i.e.*, GCG and PPS), whose deep geometry is not strictly constrained by subsurface data, have been interpreted according to the structural extensional style proposed by Brozzetti et al. (2017a). The latter is coherent with the reconstructions of the active extensional belt of the southern and central Apennines described in the literature (Barchi et al., 2007; Amicucci et al., 2008; Brozzetti et al., 2011, 2017a, 2017b; Lavecchia et al., 2017). Overall, this style is characterized by an asymmetric extension driven by a low-angle (20° to 35°) E-dipping detachment fault which represents the basal decollement of all the other extensional structures. In the model, all the faults are traced at the surface with their dip-angle as measured in outcrop and evolve downward with nearly-listric geometries to join the detachment at increasing depth from west to east. The latter represents the structurally controlled base of the seismogenic layer. The GCG (Figs 1b, 8), which crops out at low-angle and overcomes all the other east-dipping faults (in terms of both slip and associate extension), is the currently inactive break-away zone of such a detachment. The AVN and BAT (Figs 2, 8), which are the easternmost E-dipping splays, are suggested to be active and seismogenic, being possibly the causative structures of the Cluster 0 of hypocenters (Fig. 4a). Cluster 1 and Cluster 2, which are downward confined by the E-dipping detachment, confirm the activity of the W-

406 SW-dipping ROCS and MPR faults, that we consider them the main geological structures involved during the 2010-2014
407 seismic activity (Figs. 4 and 8a,a1). Further east, the 3DFM has been widened to include the W-dipping CSPT and VPP faults,
408 considered the outer seismogenic front of the extensional system. The along-strike continuity of POL and CVN is interrupted
409 by the W-dipping ROCS and MPR faults (Fig. 8c,d), coherently with the cross-cut relationships observed in the field (Fig. 2).
410 The deep geometry of POL and CVN is interrupted by the NNE-dipping AVN (Fig. 8d) which acts as the southern and basal
411 boundary of the entire active fault system.

412 Finally, the 3DFM shows that almost the whole 2010-2018 seismicity correlate with the W-dipping structures but without
413 affecting their southern termination zones. In other words, no or very few events locate south of the intersection with POL
414 and CVN faults. This latter observation suggests that although the POL and CVN did not play an active role in causing the
415 considered seismicity, they play a significant role in influencing its distribution.

416

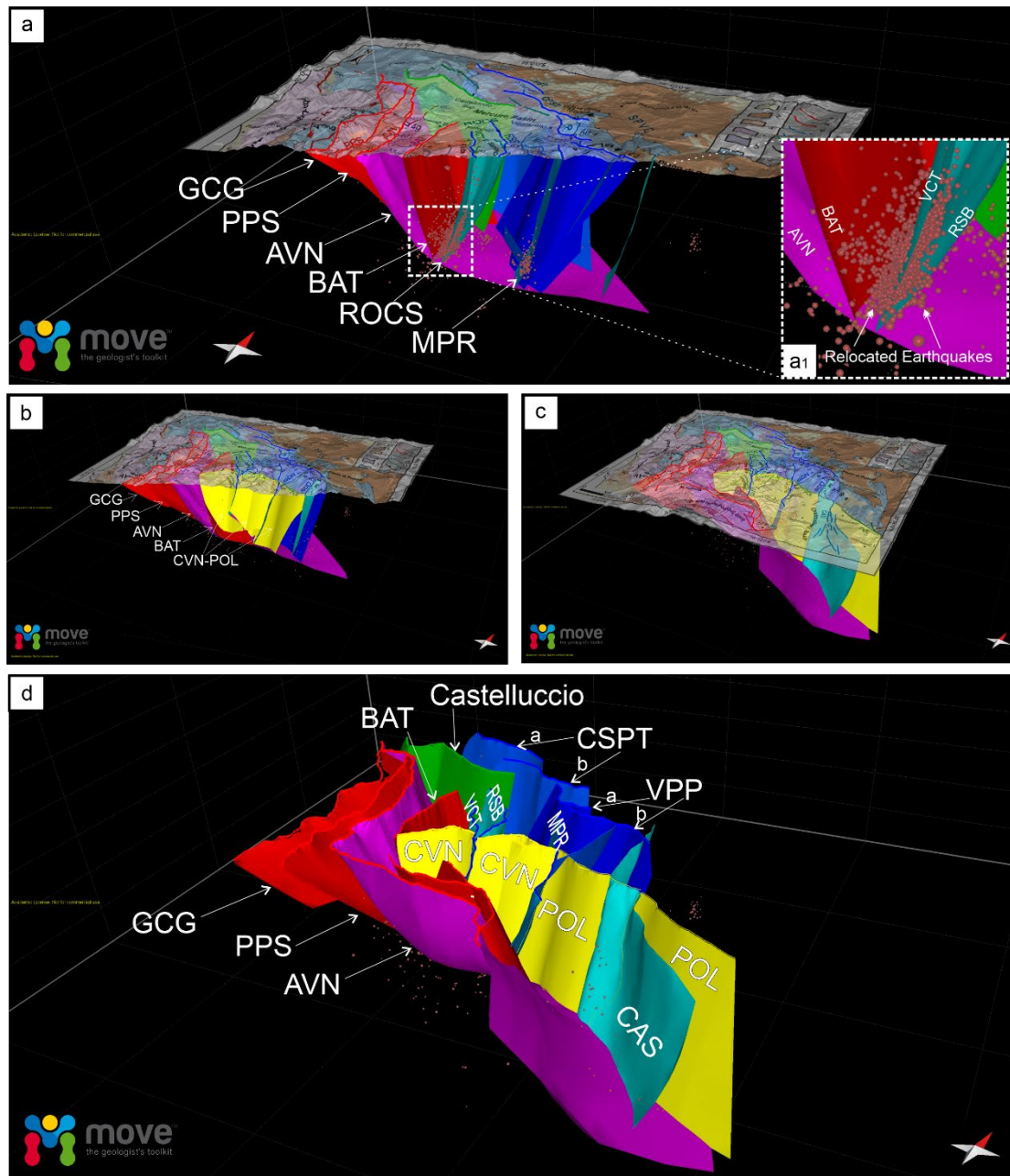


Figure 8: 3D Fault Model of the extensional system at the Calabrian-Lucanian boundary extrapolated down to ~10-12 km. In the panels (a) (b) (c) the geological-structural map (from Brozzetti et al., 2017a) is superimposed over a 10 m-resolution DEM (from Tarquini et al., 2012). The reconstruction of the fault systems is discussed in the paper. In the top panel (a), the lower right inset (a1) shown the detail of the main faults involved during the 2010-2018 seismic activity. (d) 3DFM of all extensional fault realized through the move software, for the acronyms see supplementary text 1.

424 The faults belonging to the E-NE-dipping CRFS fault set are represented in red and violet, whereas the antithetic ROCS and
425 MPR faults are shown as blue surfaces (fault acronyms as in Fig. 2). The yellow surface is the three-dimensional surface of
426 the POL and its westernmost segment (CVN) bounding, to the north, the Campotenese basin.

427

428

429 **5.4 From 3D Fault Model to expected earthquake magnitude**

430

431 Coherently with what is observed in most of the Apennine chain (D'Agostino et al., 2001; Ferranti et al., 2014; Montone and
432 Mariucci, 2016; Mariucci and Montone, 2020), the upper crustal Pollino seismicity develops in response to WSW- ENE
433 oriented extension. This is well constrained by the focal solutions of the strongest events (M_w 5.2, 25 October 2012; M_w 4.3,
434 28 May 2012, and M_w 4.0, 6 June 2014 earthquakes) and of all the $M_w \geq 3.5$ earthquakes that occurred during the 2010-2014,
435 and with the results of the geological and seismological inversion (Fig. 5). Such consistency suggests that the present stress
436 field is in continuity with the long-term one, which set up at least since the Early-Middle Pleistocene, as already suggested by
437 previous works (Papanikolaou and Roberts, 2007; Brozzetti et al. 2009; 2017a).

438 Comparing the distribution of the whole 2010-2018 seismic activity with the Late Quaternary structures mapped at the surface,
439 we maintain that the ROCS and the MPR faults are suitable as the seismogenic sources for the Mormanno (2012, M_w 5.2) and
440 Morano Calabro (2012, M_w 4.3 and 2014, M_w 4.0) earthquakes, respectively. In addition, our 3DFM allows a parameterization
441 of the sources and their seismogenic potential assessment. The map view of the W-dipping faults (Figs. 9a) depicts irregularly-
442 shaped seismogenic boxes which are delimited to the east by the fault traces (at the surface) and to the west by the branch line
443 of each fault with the base of the seismogenic layer. Some of these boxes include historical or instrumental earthquakes (Fig.
444 9b) while others are not associated with any significant event.

445 The performed 3D reconstruction allowed us to estimate the effective area extent of all the fault segments (Fig. 9c), that, when
446 inserted in the appropriate scaling relationships, provide the expected magnitude possibly releasable in case of entire rupture
447 (Fig. 9c).

448 We also computed the magnitude values obtained using the regressions as a function of the surface fault length (Fig. 9c).
449 Using six different empirical relations (Wells and Coppersmith, 1994; Wesnousky, 2008; Leonard, 2010; Stirling et al., 2013)
450 we compared the values determined, for all the investigated active normal faults (Figs. 9d,e).

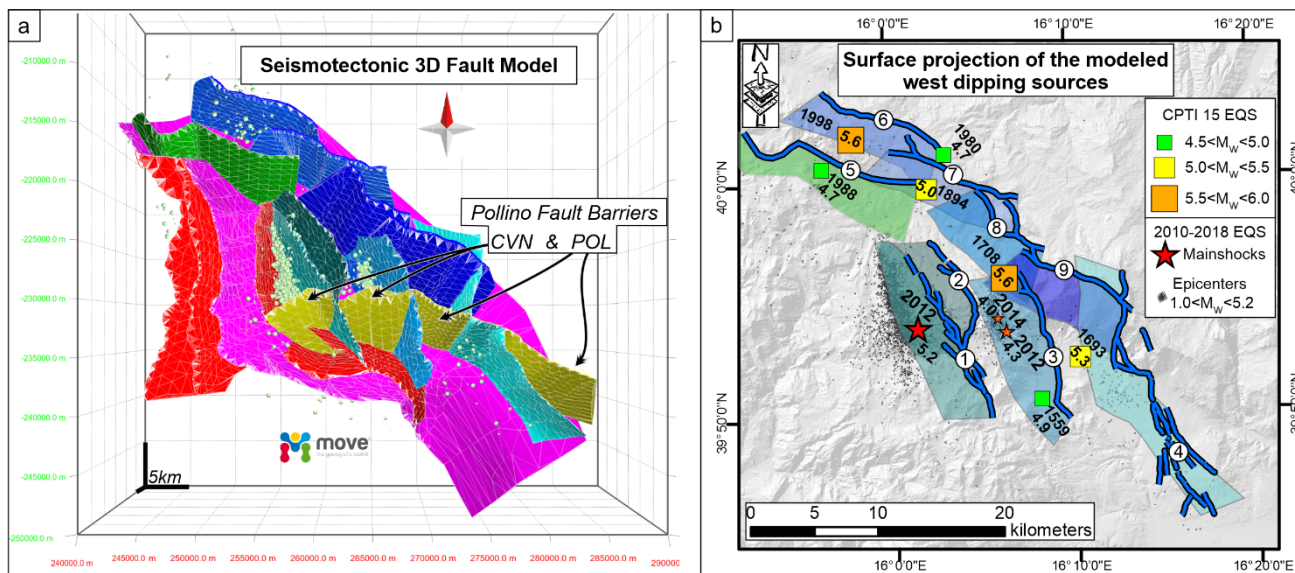
451 It is evident that, for each fault, the expected magnitude computed using fault area is lower than the one computed by using
452 fault length. The range of variation is narrower for the values computed on the ground of fault-area regressions (yellow bars
453 in Figs. 9d,e).

454 Given the significant difference in the magnitude values computed using area- or length-based scaling relationships, we
455 suggest that (where possible) the reconstruction of a 3D-fault geometry should be pursued and preferred in order to derive
456 more reliable parameters to be used (Supplementary Table 1). This is even more essential in complex extensional systems as
457 the one we investigated along the Calabrian-Lucanian border.

458 In fact, the 3DFM highlights as the areal extension of the W-dipping faults, depends on their position within the hanging wall
459 of the detachment (see sect. 5.3). This implies that faults with comparable length at the surface may have significantly different
460 areas, depending on the reached depths. The CSPT, VPP and CAS crop out at greatest distance from the GCG break-away
461 zone. Consequently, they intersect the basal detachment at the higher depth and have the maximum area extent among the W-
462 dipping fault set (Fig. 9a,d).

463 By applying the afore mentioned scaling laws (Fig. 9) to the W-dipping faults identified to be involved during the 2010-2014
464 seismic activity, we calculated the expected magnitude of $\sim M_w=6.1$ for the VCT and the RSB, and of $\sim M_w=6.2$ for the MPR.
465 Since the two faults (RSB+VCT) of the W-dipping ROCS has been interpreted to join at hypocentral depth to form a single
466 structure (thus a unique seismogenic patch was reconstructed – Fig. 10a), a value of $\sim M_w=6.4$ could be reached in the case of
467 a complete and concurrent ruptures on both the segments. The aforesaid values are sensibly higher than the magnitudes of the
468 earthquakes recorded to date in the Mercure-Campotenese area (Figs. 1b, 9b), thus suggesting that the considered faults may
469 have released only partially their seismogenic potential during historical times.

470 This inference also agrees with the distribution and evolution of the 2010-2018 seismic activity. The clusters of the relocated
471 hypocenters concentrated in the deepest parts of the ROCS and MPR faults (Fig. 6) confirming that only a portion of such
472 faults ruptured during the sequence, without the rupture reaching the surface.



Scaling Relationships for Seismic-Hazard Analysis

Fault Acronym	Area km ²	M _w (a)	M _w (b)	M _w (c)	Length km	M _w (d)	M _w (e)	M _w (f)
VCT (1)	131.07	6.1	6.2	6.1	15.16	6.5	6.7	6.8
RSB (2)	123.39	6.1	6.1	6.1	12.82	6.4	6.7	6.8
ROCS (RSB + VCT)	254.46	6.4	6.4	6.4	27.98	6.8	6.8	7.0
MPR (3)	153.01	6.2	6.2	6.2	13.33	6.4	6.7	6.8
CAS (4)	286.49	6.5	6.5	6.4	20.64	6.6	6.7	6.9
Castelluccio (5)	120.35	6.1	6.1	6.1	16.12	6.5	6.7	6.9
CSPTa (6)	164.35	6.2	6.2	6.2	11.04	6.3	6.6	6.7
CSPTb (7)	171.33	6.2	6.3	6.2	11.28	6.3	6.6	6.7
CSPT a+b	335.68	6.5	6.6	6.5	22.32	6.6	6.8	7.0
VPPa (8)	150.06	6.2	6.2	6.2	8.00	6.1	6.5	6.6
VPPb (9)	129.28	6.1	6.1	6.1	9.49	6.2	6.6	6.7
VPP a+b	279.34	6.5	6.5	6.4	17.50	6.5	6.7	6.9
SVPC (VPP+CSPT)	615.02	6.8	6.8	6.8	39.81	6.9	6.9	7.2

a Leonard 2010 (Area), dip slip

$$M_w = 4.00 + \log A$$

b Wells & Coppersmith 1994 (Area), all slip types

$$M_w = 4.07 + 0.98 \log A$$

c Wells & Copp. 1994 (Area), normal slip

$$M_w = 3.93 + 1.02 \log A$$

d Wells & Copp. 1994 (Length), normal slip

$$M_w = 5.08 + 1.16 \log L$$

e Wesnousky 2008 (Length), normal slip

$$M_w = 6.12 + 0.47 \log L$$

f Stirling et. al. 2013 (Length), normal slip

$$M_w = 5.88 + 0.88 \log L$$

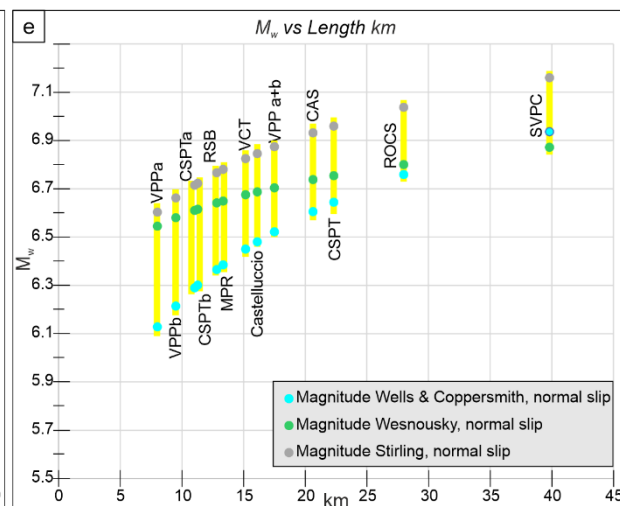
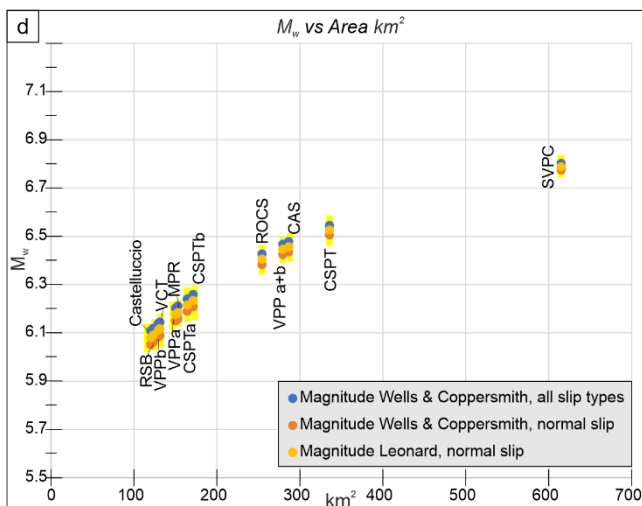


Figure 9: (a) Seismotectonic 3D Fault Model in map view. (b) Box representation of the W-dipping seismogenic faults belonging to the 3DFM with detailed segmentation pattern. Fault traces are numbered according to the table of panel (c). The associated historical earthquakes from CPTI15 v3.0 ($4.5 < M_w < 6.0$; [Rovida et al., 2020, 2021](#)) and the epicentral distribution of the 2010-2018 seismic activity occurred in the Pollino area ($1.0 < M_w < 5.2$) are also reported. (c) Expected magnitude according to scaling laws ([Wells & Coppersmith 1994](#), [Wesnowsky 2008](#), [Leonard 2010](#), [Stirling et al. 2013](#)) and calculated based on fault area (A) and length (L). (d-e) comparison of magnitude values calculated, for all the investigated active faults, using fault area- (d) and fault length- (e) based scaling relationships.

6 Discussion

6.1 Seismogenic patches activated during 2010-2014

The seismogenic patches activated on the ROCS and MPR faults during the 2010-2014 seismic sequence are considered as the reasonable approximation of the actual portion of the faults which broke during the mainshock and the sequence of the early aftershocks. We obtained them by projecting the relocated hypocenters on the reconstructed fault surface and depicting their distribution using the Kernel density geostatistical analyst, available as a tool of the ESRI ArcGIS software package. The delimitation of each seismogenic patch and its parameterization allowed us to verify the correlation between its dimensions and the magnitude released by each fault during the mainshocks.

The temporal analysis of the sequence shows that their overall extent was already well defined within the first 72 hours after the major events. Anyhow, inside the surrounding volumes, some seismicity had started before the mainshock and continued to persist constantly throughout the development of the entire sequence so that they include a percentage \geq of 70% of the whole hypocenter locations. The along-strike elongation and area extent of the patches obtained over the VCT and MPR fault surfaces can be assumed respectively as the effective Subsurface Rupture Length and Rupture Area (RLD and RA in [Fig. 10b](#), and [10c](#), respectively, according to [Wells and Coppersmith, 1994](#)) associated with the M_w 5.2 Mormanno (on VCT fault) and M_w 4.0 and 4.3 Morano Calabro (on MPR fault) earthquakes.

The parameters obtained for the VCT fault are RLD= 4.9 km and RA= 8.3 km², while RLD= 1.2 km and RA= 3.6 km² are assessed for the MPR fault. Introducing the aforesaid parameters in the appropriate scale relationships ([Fig. 10b,c](#)) we observe a good agreement between the theoretical magnitudes based on the Subsurface Rupture Length and the magnitudes of the mainshocks. The values obtained for the VCT fault (causative of the M_w 5.2 Mormanno earthquake) are M_w 5.3 whereas for the MPR fault (causative of the M_w 4.0 and 4.3 Morano Calabro earthquakes) is M_w =4.5. The magnitude calculated using the RA-based relationships provides values slightly lower than expected for the VCT ($4.9 < M_w < 5.0$) and slightly higher for the MPR ($4.5 < M_w < 4.6$). In both cases, however, the magnitude values obtained using the scale relationships differ from those observed by an amount < 0.3 .

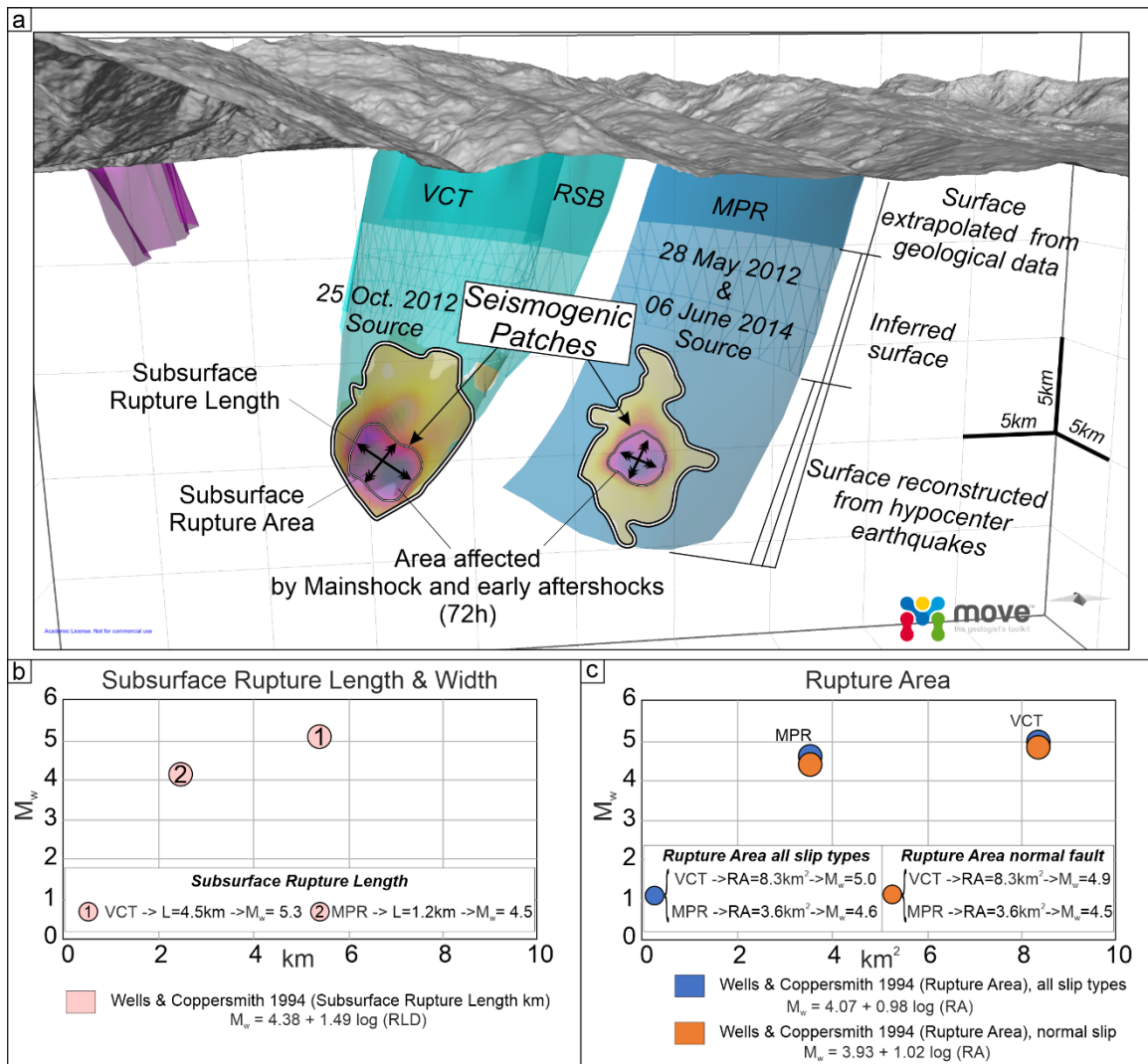


Figure 10: (a) Seismogenic patches activated during the 2010-2014 seismic activity on VCT and MPR faults. Their along-strike elongation and area extent, shown by black arrows, are assumed to be the effective subsurface rupture length and rupture area (RLD and RA, according to Wells and Coppersmith, 1994). The association of the patches' rupture with the M_w 5.2 Mormanno of the 25 October 2012 (on VCT fault) and M_w 4.3 and 4.0 Morano Calabro (on MPR fault, 28 May 2012 and 6 June 2014 respectively) earthquakes is suggested. (b) and (c) show the RLD and RA, respectively, obtained for both the VCT and MPR faults.

6.2 Possible geometric restraints to coseismic rupture propagation

The seismological dataset we used, demonstrates that the two main clusters of earthquakes of the 2010-2018 seismicity were generated by as many independent sources related to the sub-parallel, 10 to 15 km-long, ROCS and MPR faults.

Brozzetti et al. (2017a) highlighted that the above seismogenic style, characterized by a perpendicular-to-fault strike evolution of the seismic activity, is unlike from those which followed the major instrumental earthquakes recorded in the Apennine Extensional Belt of Italy in recent years, such as the Colfiorito 1997 (M_w 6.0), L'Aquila 2009 (M_w 6.3) and Norcia 2016 (M_w 6.5) events (Chiaraluce et al. 2011, 2017; Lavecchia et al., 2011, 2012a, 2016). They also speculated that this peculiar behaviour could have been controlled by the geometric fault pattern of the area, which is characterized by WSW-dipping faults bounded southward by nearly E-W pre-existing structures. These latter are genetically related to the regional-scale, long-lived, “Pollino lineament *s.l.*” (Bousquet, 1969, 1971; Ghisetti and Vezzani, 1982, 1983; Knott and Turco, 1991; Van Dijk et al., 2000) and determine the abrupt contact between the Apennine carbonate platform unit and the San Donato metamorphic core complex (Grandjaquet 1962; Servizio Geologico Nazionale, 1970; Amodio Morelli 1976). The cross-cut relationships detected in the field between the ROCS-MPR set and POL-CVN, highlighted in our 3D model, lead us to exclude the latter fault to have a present seismogenic role, as also supported by the distribution of the instrumental earthquakes which clusterized along with N-S-striking crustal volumes. However, this significant structural-geological boundary, could exert an influence on the southward propagation of the currently active seismogenic faults, driving the eastward transfer of the active extensional deformation belt. This inference is confirmed by the spatial distribution of the hypocentres of the whole 2010-2018 relocated seismicity which is confined within the CVN footwall (Fig. 8d).

537

538 7 Conclusions

539

540 We reconstructed in detail the 3D geometry and kinematics of the interconnected fault pattern responsible for the moderate-magnitude earthquakes which recently affected the Pollino area (Calabrian-Lucanian boundary).

542 The main original outcomes are summarized as follows:

543 - The geological and seismological stress tensors computed using geological- and seismological data and demonstrated that they are consistent with a uniform normal faulting regime characterized by an ENE-WSW trending, sub-horizontal σ_3 . This result confirms the coherence between the long-term and the present-day stress field and the persistence of this extensional regime at least since the Middle Pleistocene.

547

548 - The 2010-2018 seismic activity which affected the study area followed a peculiar evolution characterized by the concentration of epicenters in a series of sub-parallel ~NNW-SSE elongated clusters, independent and unconnected, which can be related to two major near-coaxial WSW-dipping faults possibly splaying from a common east-dipping basal detachment and concurrently releasing seismicity.

552

553 - The accurate hypocenter re-locations provided a seismological dataset that was correlated with the active faults mapped at the surface. The hypocenter spatial analysis allows to reconstruct the geometry (3DFM) of the seismogenic sources which released seismicity during the 2010-2014, and through 2018. This reconstruction, extrapolated down to the depth of ~10-12

556 km was the interpretative key to obtain the overall model of the Quaternary and active extension in the northern Calabria-
557 Lucania Apennines. The 3DFM model includes all the faults playing a significant role, (either direct or indirect), on the
558 seismogenesis of the study area.

559

560 - The western segment of the Pollino Fault (CVN), despite not being currently active, seems to maintain a significant
561 seismotectonic role. In fact, juxtaposing crustal sectors with different structure and composition (Apennine platform domain
562 to the north, and San Donato metamorphic core to the south) may act as a barrier to the southern propagation of the seismogenic
563 faults of the Mercure-Campotenese sector (ROCS, MPR), limiting their dimensions and seismogenic potential.

564

565 - Based on the dimension and shape of all the active faults of the Pollino area, we estimated the expected magnitudes using
566 appropriate scaling relationships. The complete rupture of individual W-dipping faults which are recognized to have been
567 causative of the 2010-2014 seismic activity is expected to release a magnitude of $\sim M_w = 6.1$ for the VCT and the RSB, and of
568 $\sim M_w = 6.2$ for the MPR. Higher values, up to $M_w = 6.4$, could be reached in the case of the complete and concurrent rupture on
569 both RSB and VCT. The estimated values exceed the magnitudes of the associate earthquakes which struck the area to date,
570 leading to hypothesize that the aforesaid faults released only partially their seismogenic potential.

571

572 - The delimitation of the fault patches involved during 2010-2014, and their geometrical parameterization, support the
573 consistence between the theoretical magnitudes based on the Subsurface Rupture Length and the magnitudes of the
574 mainshocks.

575 The estimates provided, for the VCT fault (which released the M_w 5.2 Mormanno earthquake) a $M_w = 5.3$, and for the MPR
576 fault (which released the M_w 4.0 and 4.3 Morano Calabro earthquakes) a $M_w = 4.5$. The magnitudes calculated using the
577 relationships based on the Subsurface Rupture Area ($M_w \sim 5.0$ for the VCT and $M_w \sim 4.6$ for the MPR), show slightly greater
578 deviation from the observed values.

579

580 This study pointed out as even in the case of low-to-moderate seismic activity, like the Pollino 2010-2014 one, the approach
581 based on the three-dimensional reconstruction of the Quaternary fault surfaces (both directly involved and neighboring in the
582 extensional system), represents a real breakthrough in the seismotectonic analysis and, ultimately, in the cognitive path that
583 leads to a better assessment of the seismic hazard of a tectonically active area.

584

585 **Author contribution:** DC, FB conceived and conducted the study. FB, DC, FF, SB wrote the manuscript. DC developed the
586 3D structural-geological model through Move software. DC, SB, FF did GIS analysis and mapping. DC, FB, SB performed
587 the fieldwork. CT, DP, BO, RdN, handled the seismological analysis. FF did the geological and seismological stress-tensor
588 inversion. DC performed the calculation of the expected magnitudes. DC prepared the figures. GL, SB, FB, RdN reviewed the
589 figures. DC, SB prepared the GIS geological database. All authors reviewed the final version of the manuscript.

590

591 **Competing interests:** The authors declare no conflict of interest.

592

593 **Disclaimer.** Publisher's note: Copernicus Publications remains neutral with regard to jurisdictional claims in published maps
594 and institutional affiliations.

595

596 **Special issue statement.** This article is part of the special issue "Tools, data and models for 3-D seismotectonics: Italy as a key
597 natural laboratory".

598

599 **Acknowledgements:**

600 The authors are grateful to Petroleum Experts, who provided the Move, 2019.1 suite software license. We are grateful to the
601 Editor Massimiliano Porreca, to Giovanni Barreca and to an anonymous reviewer for improving the manuscript with their
602 review.

603

604 **Financial support.** Funding was from the DPC-INGV PROJECTS-S1 2014-2015 UR-Unich, resp. F. Brozzetti and from
605 DiSPUTer Department research funds to F. Brozzetti. This research was also supported by PRIN 2017 (2017KT2MKE) funds
606 from the Italian Ministry of Education, University and Research (P.I. Giusy Lavecchia).

607

608 **Review statement.** This paper was edited by Massimiliano Porreca and reviewed by Giovanni Barreca and by an anonymous
609 referee.

610

611 **References**

612

613 Allmendinger, R. W., Cardozo, N., and Fisher, D.: Structural geology algorithms: Vectors and tensors in structural geology:
614 Cambridge University Press (book to be published in early 2012) 2012.

615

616 Amicucci, L., Barchi, M.R., Montone, P., and Rubilani, N.: The Vallo di Diano and Auletta extensional basins in the southern
617 Apennines (Italy): a simple model for a complex setting, Terra Nova, 20, 475-482, [https://doi.org/10.1111/j.1365-](https://doi.org/10.1111/j.1365-3121.2008.00841.x)
618 [3121.2008.00841.x](https://doi.org/10.1111/j.1365-3121.2008.00841.x), 2008.

619

620 Amodio Morelli, L., Bonardi, G., Colonna, V., Dietrich, D., Giunta, G., Ippolito, F., Liguori, V., Lorenzoni, S., Paglionico,
621 A., Perrone, V., Piccarreta, G., Russo, M., Scandone, P., Zanettin-Lorenzoni, E., and Zuppetta, A.: L'Arco calabro peloritano
622 nell'orogene appenninico-maghrebide, Mem. Soc. Geol. It. 17, 1-60, 1976.

623

624 Angelier, J., and Mechler, P. : Sur une méthode graphique de recherche des contraintes principales également utilisable en
625 tectonique et en séismologie: la méthode des dièdres droits, B. Soc. Géol. Fr., 7, 1309–1318, 1977.

626

627 Arrigo, G., Roumelioti, Z., Benetatos, C., Kiratzi, A., Bottari, A., Neri, G., Termini, D., Gorini, A., and Marcucci, S. : A source
628 study of the 9 September 1998 (Mw 5.6) Castelluccio Earthquakes in Southern Italy using Teleseismic and strong motion data,
629 Nat. Hazards 00, 1-16, doi:10.1007/s1001 1069-1005-4644-1001, 2005.

630

631 Ascione, A., Mazzoli, S., Petrosino, P., and Valente, E.: A decoupled kinematic model for active normal faults: insights from
632 the 1980, MS=6.9 Irpinia earthquake, southern Italy, GSA Bull 125, 1239-1259, doi:10.1130/B30814.1, 2013.

633

634 Barchi, M. R., De Feyter, A., Magnani, M. B., Minelli, G., Piali, G., and Sotera, B. M.: Extensional tectonics in the northern
635 Apennines (Italy): Evidence from the CROP03 deep seismic reflection line, Mem. Soc. Geol. Ital., 52, 527– 538, 1998.

636

637 Barchi, M., Lavecchia, G., Galadini, F., Messina, P., Michetti, A. M., Peruzza, L., Pizzi, A., Tondi, E., and Vittori, E.: Sintesi
638 delle conoscenze geologiche sulle faglie responsabili dei terremoti maggiori in Italia Centrale: Parametrizzazione ai fini della
639 caratterizzazione della pericolosità sismica, Gruppo Naz. per la Difesa dai Terremoti, CNR, Rome, 1999.

640

641 Barchi, M., Amato, A., Cippitelli, G., Merlini, S., and Montone, P.: Extensional tectonics and seismicity in the axial zone of
642 the southern Apennines, Boll. Soc. Geol. It. (Ital. J. Geosci.) 7, 47-56, 2007.

643

644 Barchi, M.R., Carboni, F., Michele, M., Ercoli, M., Giorgetti, C., Porreca, M., Azzaro, S., and Chiaraluca, L.: The influence
645 of subsurface geology on the distribution of earthquakes during the 2016–2017 Central Italy seismic sequence,
646 Tectonophysics, 807, 228797, <https://doi.org/10.1016/j.tecto.2021.228797>, 2021.

647

648 Bello S., de Nardis R., Scarpa R., Brozzetti F., Cirillo D., Ferrarini F., di Lieto B., Arrowsmith R. J., and Lavecchia G.: Fault
649 Pattern and Seismotectonic Style of the Campania-Lucania 1980 Earthquake (Mw 6.9, Southern Italy): New Multidisciplinary
650 Constraints, Frontiers in Earth Science, 8, 652, <https://doi.org/10.3389/feart.2020.608063>, 2021a.

651

652 Bello, S., Scott, C. P., Ferrarini, F., Brozzetti, F., Scott, T., Cirillo, D., de Nardis R., Arrowsmith R. J., and Lavecchia G.:
653 High-resolution surface faulting from the 1983 Idaho Lost River Fault Mw 6.9 earthquake and previous events. Sci. Data 8,
654 68, 1-20, <https://doi.org/10.1038/s41597-021-00838-6>, 2021b.

655

656 Bello, S., Andrenacci, C., Cirillo, D., Scott, T., Brozzetti, F., Arrowsmith R. J., and Lavecchia G.: High-detail fault
657 segmentation: Deep insight into the anatomy of the 1983 Borah Peak earthquake rupture zone (Mw 6.9, Idaho, USA),
658 Lithosphere, 8100224, <https://doi.org/10.2113/2021/8100224>, 2021c.

659

660 Blumetti, A. M., Esposito, E., Ferrelì, L., Michetti, A. M., Porfido, S., Serva, L., et al.: New data and the reinterpretation of
661 the November 23, 1980, M 6.9, Irpinia-Lucania earthquake (Southern Apennines) coseismic surface effects, Spec. Issue Studi
662 Geologici Camerti 2, 19-27, 2002.

663

664 Bonini, L., Toscani, G., and Seno S. : Three-dimensional segmentation and different rupture behavior during the 2012 Emilia
665 seismic sequence (Northern Italy), Tectonophysics, 630, 33-42, 10.1016/j.tecto.2014.05.006, 2014.

666

667 Bousquet, J.C., and Guerey, P. : Quelques Phénomènes de Néotectonique dans l'Apennin Calabro-Lucanien et Leurs
668 Conséquences Morphologiques. Rev. Géogr. Phys. Géol. Dynam 10, 225-238, 1969.

669

670 Bousquet, J.C.: La tectonique tangentielle des series calcareo-dolomitiques du nord-est de l'Apennin Calabro-Lucanien (Italie
671 Méridionale). Geol. Rom. X, 23-52, 1971.

672

673 Brozzetti, F., and Lavecchia, G.: Seismicity and related extensional stress field: the case of the Norcia Seismic Zone (Central
674 Italy), Ann. Tectonicae, 8(1), 36-57, 1994.

675

676 Brozzetti, F., Lavecchia, G., Mancini, G., Milana G. and Cardinali, M.: Analysis of the 9 September 1998 Mw 5.6 Mercure
677 earthquake sequence (southern Apennines, Italy): a multidisciplinary approach, Tectonophysics, 476, 210-225.
678 <https://doi.org/10.1016/j.tecto.2008.12.007>, 2009.

679

680 Brozzetti, F.: The Campania-Lucania extensional fault system (southern Italy): a suggestion for a uniform model of active
681 extension in the Italian Apennines, Tectonics, 30 (5), 1-26, TC5009, <http://dx.doi.org/10.1029/2010TC002794>, 2011.

682

683 Brozzetti, F., Cirillo, D., Liberi, F., Faraca, E. and Piluso, E.: The Crati Valley Extensional System: field and subsurface
684 evidences, Rend. Online Soc. Geol. It., Vol. 21 (2012), pp. 159-161.

685

686 Brozzetti, F., Cirillo, D., de Nardis, R., Cardinali, M., Lavecchia, G., Orecchio, B., Presti D., and Totaro, C.: Newly identified
687 active faults in the Pollino seismic gap, southern Italy, and their seismotectonic significance, J. Struct. Geol., 94, 13-31,
688 <https://doi.org/10.1016/j.jsg.2016.10.005>, 2017a.

689

690 Brozzetti, F., Cirillo, D., Liberi, F., Piluso, E., Faraca, E., De Nardis, R., and Lavecchia, G.: Structural style of Quaternary
691 extension in the Crati Valley (Calabrian Arc): Evidence in support of an east-dipping detachment fault, *It. Journ. of Geosci.*,
692 136(3), 434-453, <https://doi.org/10.3301/IJG.2017.11>, 2017b.

693

694 Brozzetti, F., Cirillo, D., and Luchetti, L.: Timing of Contractional Tectonics in the Miocene Foreland Basin System of the
695 Umbria Pre-Appennines (Italy): An Updated Overview, *Geosciences* 2021, 11, 97.
696 <https://doi.org/10.3390/geosciences11020097>, 2021.

697

698 Caiazzo, C., Giovine, B., Ortolani, F., Pagliuca, S., Schiattarella, M., Barchi and Vitale, C.: Genesi ed evoluzione strutturale
699 della depressione tettonica dell'alta valle del Fiume Sele (Appennino Campano Lucano), *Stud. Geol. Camerti*, 1992(1), 245–
700 255, 1992.

701

702 Calamita, F., Pizzi, A., and Roscioni, M.: I fasci di faglie recenti ed attive di M. Vettore - M. Bove e di M. Castello - M.
703 Cardosa (Appennino Umbro-Marchigiano), In *Studi Geologici Camerti*; Università di Camerino: Camerino, Italy, 81-95, 1992;
704 Available online: <http://193.204.8.201:8080/jspui/handle/1336/552>, last access: 19 April 2021.

705

706 Castaldo, R., de Nardis, R., De Novellis, V., Ferrarini, F., Lanari, R., Lavecchia, G., et al.: Coseismic stress and strain field
707 changes investigation through 3-D Finite Element modeling of DInSAR and GPS measurements and geological/seismological
708 data: the l'aquila (Italy) 2009 earthquake case study, *J. Geophys. Res. Solid Earth* 123, 4193-4222,
709 <https://doi.org/10.1002/2017JB014453>, 2018.

710

711 Castello, B., Selvaggi, G., Chiarabba, C., and Amato, A.: CSI Catalogo della sismicità italiana 1981-2002, versione 1.1. Roma:
712 INGV-CNT, 2006, <https://csi.rm.ingv.it/>, last access: 19 April 2021.

713

714 Cello, G., Tondi, E., Micarelli, L., and Mattioni L.: Active tectonics and earthquake sources in the epicentral area of the 1857
715 Basilicata earthquake (southern Italy), *Journal of Geodynamics*, 36, 1-2, 37-50, [https://doi.org/10.1016/S0264-3707\(03\)00037-](https://doi.org/10.1016/S0264-3707(03)00037-1)
716 [1](https://doi.org/10.1016/S0264-3707(03)00037-1), 2003.

717

718 Cheloni, D., D'Agostino, N., Selvaggi, G., Avallone, A., Fornaro, G., Giuliani, R., Reale, D., Sansosti, E., and Tizzani, P.,:
719 Aseismic transient during the 2010–2014 seismic swarm: evidence for longer recurrence of $M_l \geq 6.5$ earthquakes in the Pollino
720 gap (Southern Italy)?, *Sci. Rep.*, 7(576), <https://doi.org/10.1038/s41598-017-00649-z>, 2017.

721

722 Chiaraluce, L., Amato, A., Cocco, M., Chiarabba, C., Selvaggi, G., Di Bona, M., Piccinini, D., Deschamps, A., Margheriti, L.,
 723 Courboux, F., and Ripepe, M.: Complex normal faulting in the Apennines thrust-and-fold belt: The 1997 seismic sequence
 724 in Central Italy, *Bull. Seismol. Soc. Am.* 94, 99-116, <https://doi.org/10.1785/0120020052>, 2004.
 725
 726 Chiaraluce, L., Barchi, M.R., Collettini, C., Mirabella, F., and Pucci, S.: Connecting seismically active normal faults with
 727 Quaternary geological structures: the Colfiorito 1997 case history (Northern Apennines, Italy), *Tectonics* 24, TC1002, 1-16,
 728 <https://doi.org/10.1029/2004TC001627>, 2005.
 729
 730 Chiaraluce, L., Valoroso, L., Piccinini, D., Di Stefano, R., and De Gori, P.: The anatomy of the 2009 L'Aquila normal fault
 731 system (central Italy) imaged by high resolution foreshock and aftershock locations, *J. Geophys. Res.* 116, no. B12,
 732 <https://doi.org/10.1029/2011JB008352>, 2011.
 733
 734 Chiaraluce, L., Di Stefano, R., Tinti, E., Scognamiglio, L., Michele, M., Casarotti, E., Cattaneo, M., De Gori, P., Chiarabba,
 735 C., Monachesi, G., Lombardi, A., Valoroso, L., Latorre, D., and Marzorati, S.: The 2016 Central Italy Seismic Sequence: A
 736 First Look at the Mainshocks, Aftershocks, and Source Models, *Seismological Research Letters*, 88(3), 757-771,
 737 <https://doi.org/10.1785/0220160221>, 2017.
 738
 739 Cifelli, F., Rossetti, F., and Mattei, M.: The architecture of brittle postorogenic extension: Results from an integrated structural
 740 and paleomagnetic study in north Calabria (southern Italy), *GSA Bull.*, **119**, 221-239, 2007.
 741
 742 Cinque, A., Patacca, E., Scandone, P., and Tozzi, M.: Quaternary kinematic evolution of the southern apennines. relationship
 743 between surface geological features and lithospheric structures, *Ann. Geofisc* 36, 249-260. <https://doi.org/10.4401/ag-4283>,
 744 1993.
 745
 746 Cinque, A., Ascione, A., and Caiazza, C.: Distribuzione spaziotemporale e caratterizzazione della fagliazione quaternaria in
 747 Appennino meridionale, in *Le Ricerche del GNDT nel Campo Della Pericolosità Sismica (1996-1999)*, edited by F. Galadini,
 748 C. Meletti, and A. Rebez, 397 pp., CNR, Gruppo Naz. per la Difesa dai Terremoti, Rome, 2000.
 749
 750 Cinti, F. R., Cucci, L., Pantosti, D., D'Addezio, G., and Meghraoui, M.: A major seismogenic fault in a 'silent area': the
 751 Castrovillari fault (Southern Apennines, Italy), *Geophysical Journal International*, 130(3), 595-605, 1997. [https://www.earth-](https://www.earth-prints.org/bitstream/2122/12031/1/text.pdf)
 752 [prints.org/bitstream/2122/12031/1/text.pdf](https://www.earth-prints.org/bitstream/2122/12031/1/text.pdf), last access: 19 April 2021.
 753
 754 Cinti, F. R., Moro, M., Pantosti, D., Cucci, L., and D'Addezio, G.: New constraints on the seismic history of the Castrovillari
 755 fault in the Pollino gap (Calabria, southern Italy), *J. Seismol.*, 6, 199-217. <https://doi.org/10.1023/A:1015693127008>, 2002.

756

757 Cirillo, D.: Digital Field Mapping and Drone-Aided Survey for Structural Geological Data Collection and Seismic Hazard
758 Assessment: Case of the 2016 Central Italy Earthquakes, *Applied Sciences*, 10, 5233. <https://doi.org/10.3390/app10155233>,
759 2020.

760

761 D'Agostino, N., Giuliani, R., Mattone, M., Bonci, L.: Active crustal extension in the central Apennines (Italy) inferred from
762 GPS measurements in the interval 1994-1999, *Geophysical Research Letters*, 28(10), 2121-2124, 10.1029/2000GL012462,
763 2001.

764

765 D'Agostino, N.: Complete seismic release of tectonic strain and earthquake recurrence in the Apennines (Italy), *Geophys. Res.*
766 *Lett* 41, 1155-1162, <https://doi.org/10.1002/2014GL059230>, 2014.

767

768 D'Alessandro, A., Gervasi, A., and Guerra, I.: Evolution and strengthening of the Calabrian regional seismic network. *Adv.*
769 *Geosciences* 36, 11-16, 2013. <https://adgeo.copernicus.org/articles/36/11/2013/adgeo-36-11-2013.pdf>, last access: 19 April
770 2021.

771

772 D'Argenio, B.: L'Appennino Campano Lucano. Vecchi e nuovi modelli geologici tra gli anni sessanta e gli inizi degli anni
773 ottanta. *Mem. Soc. Geol. It.* 41, 3-15, 1992.

774

775 Delaunay, B.: Sur la sphere vide, *Bull. Acad. Sci. USSR(VII)*, Classe Sci. Mat. Nat., 793-800, 1934.

776

777 Delvaux, D., and Sperner, B.: New aspects of tectonic stress inversion with reference to the TENSOR program. In: *New*
778 *Insights into Structural Interpretation and Modelling* (D.A. Nieuwland, ed.), *J. Geol. Soc. London Spec. Publ.*, 212, 75-100,
779 2003.

780

781 Delvaux, D., and Barth, A.: African stress pattern from formal inversion of focal mechanism data, *Tectonophysics*, 482, 105-
782 128, 2010.

783

784 Devoti, R., Esposito, A., Pietrantonio, G., Pisani, A. R., and Riguzzi, F.: Evidence of large-scale deformation patterns from
785 GPS data in the Italian subduction boundary, *Earth Planet Sci. Lett* 311, 230–241. Doi:10.1016/j.epsl.2011.09.034, 2011.

786

787 De Matteis, R., Convertito, V., Napolitano, F., Amoroso, O., Terakawa, T., and Capuano, P.: Pore fluid pressure imaging of
788 the Mt. Pollino region (southern Italy) from earthquake focal mechanisms, *Geophysical Research Letters*, 48,
789 e2021GL094552. <https://doi.org/10.1029/2021GL094552>, 2021.

790

791 Di Bucci, D., Buttinelli, M., D'Ambrogio, C., and Scrocca, D., and the RETRACE-3D Working Group: The RETRACE-3D
792 multi-data and multi-expertise approach towards the construction of a 3D crustal model for the 2016-2018 Central Italy seismic
793 sequence, *Boll. Geof. Teor. Appl.* DOI 10.4430/bgta0343, 2021.

794

795 Elter, P., Giglia, G., Tongiorgi, M., and L. Trevisan, L.: Tensional and compressional areas in the recent (Tortonian to present)
796 evolution of the northern Apennines, *Boll. Geofis. Teor. Appl.*, 17, 3-18, 1975.

797

798 Ercoli, M., Pauselli, C., Forte, E., Frigeri, A., and Federico, C.: The Mt. Pollino Fault (southern Apennines, Italy): GPR
799 signature of Holocene earthquakes in a “silent” area. In: *Advanced Ground Penetrating Radar (IWAGPR)*, 2013 7th
800 International Workshop. IEEE, pp. 1-6. <http://dx.doi.org/10.1109/IWAGPR.2013.6601510>, 2013.

801

802 Ercoli, M., Cirillo, D., Pauselli, C., Jol, H. M., and Brozzetti, F.: GPR signature of Quaternary faulting: a study from the Mt.
803 Pollino region, southern Apennines, Italy, *Solid Earth*, <https://doi.org/10.5194/se-2021-75>, 2021.

804

805 Faure Walker, J. P., Roberts, G. P., Cowie, P. A., Papanikolaou, I., Michetti, A. M., Sammonds, P., et al.: Relationship between
806 topography, rates of extension and mantle dynamics in the actively-extending Italian Apennines, *Earth Planet Sci. Lett* 325–
807 326, 76–84. doi:10.1016/j.epsl.2012.01.028, 2012.

808

809 Ferranti, L., Palano, M., Cannavò, F., Mazzella, M. E., Oldow, J. S., Gueguen, E., et al.: Rates of geodetic deformation across
810 active faults in southern Italy, *Tectonophysics* 621, 101–122. doi:10.1016/j.tecto.2014.02.007, 2014.

811

812 Ferranti, L., Milano, G., and Pierro, M., Insights on the seismotectonics of the western part of northern Calabria (southern
813 Italy) by integrated geological and geophysical data: coexistence of shallow extensional and deep strike-slip kinematics,
814 *Tectonophysics*, 721, 372–386, <https://doi.org/10.1016/j.tecto.2017.09.020>, 2017.

815

816 Ferrarini, F., Lavecchia, G., de Nardis, R., and Brozzetti, F.: Fault geometry and active stress from earthquakes and field
817 geology data analysis: the Colfiorito 1997 and L'Aquila 2009 cases (central Italy), *Pure Appl. Geoph.*, 172 (5), 1079-1103,
818 <https://doi.org/10.1007/s00024-014-0931-7>, 2015.

819

820 Ferrarini, F., Boncio, P., de Nardis, R., Pappone, G., Cesarano, M., Aucelli, P.P.C., and Lavecchia, G.: Segmentation pattern
821 and structural complexities in seismogenic extensional settings: The North Matese Fault System (Central Italy), *J. Struct.*
822 *Geol.*, 95, 93-112, <http://dx.doi.org/10.1016/j.jsg.2016.11.006>, 2017.

823

824 Ferrarini, F., de Nardis, R., Brozzetti, F., Cirillo, D., Arrowsmith, JR. and Lavecchia, G.: Multiple Lines of Evidence for a
825 Potentially Seismogenic Fault Along the Central-Apennine (Italy) Active Extensional Belt—An Unexpected Outcome of the
826 MW6.5 Norcia 2016 Earthquake, *Front. Earth Sci.* 9:642243. doi: 10.3389/feart.2021.642243, 2021.

827

828 Filice, F., Liberi, F., Cirillo, D., Pandolfi, L., Marroni, M., and Piluso E.: Geology map of the central area of Catena Costiera:
829 insights into the tectono-metamorphic evolution of the Alpine belt in Northern Calabria, *Journal of Maps*, 11(1), 114-125,
830 <https://doi.org/10.1080/17445647.2014.944877>, 2015.

831

832 Filice, F., and Seeber, L.: The Culmination of an Oblique Time-Transgressive Arc Continent Collision: The Pollino Massif
833 Between Calabria and the Southern Apennines, Italy, *Tectonics*, 38(1), 3261-3280. <https://doi.org/10.1029/2017TC004932>,
834 2019.

835

836 Frepoli, A., Cinti, R., Amicucci, L., Cimini, G.B., De Gori, P., and Pierdominici, S.: Pattern of seismicity in the Lucanian
837 Apennines and foredeep (Southern Apennines) from recording by SAPTEX temporary array, *Annal. Geophys.*, 48, 1035-1054,
838 2005. <https://www.earth-prints.org/bitstream/2122/1131/6/manuscript.pdf> , last access: 19 April 2021.

839

840 Frohlich, C.: Display and quantitative assessment of distributions of earthquakes focal mechanisms, *Geophys. J. Int.* 144, 300-
841 308, 2001.

842

843 Gafarov, K., Ercoli, M., Cirillo, D., Pauselli, C., and Brozzetti, F.: Extending surface geology data through GPR prospections:
844 Quaternary faulting signature from the Campotenese area (Calabria-Italy), 17th International Conference on Ground
845 Penetrating Radar, GPR, 8441611, 2018.

846

847 Galadini, F., and P. Galli: Active tectonics in the Central Apennines (Italy): Input data for seismic hazard assessment, *Nat.*
848 *Hazards*, 22, 225–268, doi:10.1023/A:1008149531980, 2000.

849

850 Galli, P., and Peronace, E.: New paleoseismic data from the Irpinia fault. A different seismogenic perspective for the southern
851 Apennines, *Earth Sci. Rev.* 136, 175-201, <https://doi.org/10.1016/j.earscirev.2014.05.013>, 2014.

852

853 Galli, P.: Recurrence times of central-southern Apennine faults (Italy): Hints from paleoseismology, *Terra Nova*, 32, 399-407,
854 <https://doi.org/10.1111/ter.12470>, 2020.

855

856 Gephart, J.W., and Forsyth, D.W.: An improved method for determining the regional stress tensor using earthquake focal
857 mechanism data: application to the San Fernando earthquake sequence, *J. Geophys. Res.*, 89, 9305-9320, 1984.

858

859 Ghisetti, F., and Vezzani, L.: Strutture tensionali e compressive indotte da meccanismi profondi lungo la linea del Pollino
860 (Appennino meridionale), Boll. Soc. Geol. It. 101, 385-440, 1982.

861

862 Ghisetti, F., and Vezzani, L.: Structural Map of Mt. Pollino (Southern Italy), 1:50.000 Scale, SELCA, Firenze, 1983.

863

864 Giano, S. I., and Martino, C.: Assetto morfotettonico e morfostratigrafico di alcuni depositi continentali pleistocenici del bacino
865 del Pergola–Melandro (Appennino Lucano). Quaternario 16 (2), 289–297, 2003.

866

867 Gràcia, E., Grevemeyer, I., Bartolomé, R. et al. : Earthquake crisis unveils the growth of an incipient continental fault system.
868 Nat. Commun. 10, 3482, <https://doi.org/10.1038/s41467-019-11064-5>, 2019.

869

870 Grandjacquet, C.: Données nouvelles sur la tectonique tertiaire des massif Calabro-Lucaniens. Bull. Soc. Geol. Fr. 7ème série
871 4, 695-706, 1962.

872

873 Guerra, I., Harabaglia, P., Gervasi, A., and Rosa, A.B.: The 1998–1999 Pollino (Southern Apennines, Italy) seismic crisis:
874 tomography of a sequence, Ann. Geophys. 48, 995-1007, <https://doi.org/10.4401/ag-3249>, 2005.

875

876 Guidoboni E., Ferrari G., Mariotti D., Comastri A., Tarabusi G., Sgattoni G., and Valensise G.: CFTI5Med, Catalogo dei Forti
877 Terremoti in Italia (461 a.C.-1997) e nell'area Mediterranea (760 a.C.-1500), Istituto Nazionale di Geofisica e Vulcanologia
878 (INGV), <http://storing.ingv.it/cfti/cfti5/>, 2018.

879

880 Guidoboni, E., Ferrari, G., Tarabusi, G., Sgattoni, G., Comastri, A., Mariotti, D., Ciuccarelli, C., Bianchi, M.G., and Valensise
881 G.: CFTI5Med, the new release of the catalogue of strong earthquakes in Italy and in the Mediterranean area, Scientific Data
882 6, article number: 80, doi: <https://doi.org/10.1038/s41597-019-0091-9>, 2019.

883

884 Heidbach, O., Tingay, M., Barth, A., Reinecker, J., Kurfeß, D., and Müller, B.: Global crustal stress pattern based on the world
885 stress map database release 2008, Tectonophysics 482, 3-15, <https://doi.org/10.1016/j.tecto.2009.07.023>, 2010.

886

887 Hippolite, J.C., Angelier, J., and Barrier, E.: Compressional and extensional tectonics in an arc system; example of the Southern
888 Apennines, J. Struct. Geol. 17, 1725–1740, [https://doi.org/10.1016/0191-8141\(95\)00066-M](https://doi.org/10.1016/0191-8141(95)00066-M), 1995.

889

890 Husen, S., and Smith, R.: Probabilistic earthquake location in three-dimensional velocity models for the Yellowstone National
 891 Park region, Wyoming, *Bull. Seism. Soc. Am.* 94 (6), 880-896, 2004.
 892 <https://uusatrg.utah.edu/PAPERS/husen2004probeqreloc.pdf>, last access: 19 April 2021.
 893
 894 Iannace, A., D'Errico, M., and Vitale, S.: Carta Geologica dell'area compresa tra Maratea, Castrovillari e Sangineto. In: Vitale,
 895 S., Iannace, A. (Eds.), *Analisi Dello Strain Finito in 3D Dell'Unità Pollino-Ciagola (Confine Calabro-lucano, Italia*
 896 *Meridionale)*, Studi Geologici Camerti, Nuova Serie, 2, 153-167 (ISSN: 0392-0631), 2004.
 897
 898 Iannace, A., Garcia Tortosa, F.J., and Vitale, S.: The Triassic metasedimentary successions across the boundary between
 899 Southern Apennines and Calabria–Peloritani Arc (Northern Calabria, Italy), *Geol. J.*, 40, 155–171.
 900 <https://doi.org/10.1002/gj.1001>, 2005.
 901
 902 Iannace, A., Vitale, S., D'Errico, M., Mazzoli, S., Di Staso, A., Macaione, E., Messina, A., Reddy, S.M., Somma, R.,
 903 Zamparelli, V., Zattin, M., and Bonardi, G.: The carbonate tectonic units of northern Calabria (Italy): a record of Apulian
 904 palaeomargin evolution and Miocene convergence, continental crust subduction, and exhumation of HP–LT rocks, *J. Geol.*
 905 *Soc. Lond.* 164, 1165-1186. <https://doi.org/10.1144/0016-76492007-017>, 2007.
 906
 907 Ietto, A., and Barilaro, A.M.: L'Unità di San Donato quale margine deformato Cretacico-Paleogene del bacino di Lagonegro
 908 (Appennino Meridionale-Arco Calabro), *Boll. Soc. Geol. It.* 112, 477-496, 1993.
 909
 910 ISIDe Working Group: Italian Seismological Instrumental and Parametric Database (ISIDe). Istituto Nazionale di Geofisica e
 911 Vulcanologia (INGV), <https://doi.org/10.13127/ISIDE>, 2007, last access: 19 April 2021.
 912
 913 Johnson, K., Nissen, E., Saripalli, S., Arrowsmith, J.R., McGarey, P., Scharer, K., Williams, P., Blisniuk, K.: Rapid mapping
 914 of ultrafine fault zone topography with structure from motion, *Geosphere*, 10, 969–986, 2014.
 915
 916 Klin, P., Laurenzano, G., Romano, M.A., Priolo, E., Martelli, L.: ER3D: a structural and geophysical 3-D model of central
 917 Emilia-Romagna (northern Italy) for numerical simulation of earthquake ground motion, *Solid Earth*, 743, 10:931–949.
 918 <https://doi.org/10.5194/se-10-931-2019>. 2019.
 919
 920 Knott, S.D., and Turco, E.: Late cenozoic kinematics of the Calabrian arc, southern Italy. *Tectonics* 10 (6), 1164-1172, 1991.
 921

922 Lavecchia, G., Brozzetti, F., Barchi, M., Menichetti, M., and Keller, J. V. A.: Seismotectonic zoning in east-central Italy
 923 deduced from an analysis of the Neogene to present deformations and related stress fields, *Geol. Soc. Am. Bull.* 106, 1170-
 924 1120, doi:10.1130/0016, [https://doi.org/10.1130/0016-7606\(1994\)106%3C1107:SZIECI%3E2.3.CO;2](https://doi.org/10.1130/0016-7606(1994)106%3C1107:SZIECI%3E2.3.CO;2), 1994.

925

926 Lavecchia, G., Boncio, P., Brozzetti, F., De Nardis, R., Di Naccio, D., Ferrarini, F., Pizzi, A., and Pomposo, G.: The April
 927 2009 L'Aquila (central Italy) seismic sequence (Mw 6.3): a preliminary seismotectonic picture, *Recent Prog. Earthquake Geol.*
 928 2011, 1-17, ISBN: 978-1-60876-147-0, 2011.

929

930 Lavecchia, G., Ferrarini, F., Brozzetti, F., de Nardis, R., Boncio, P., and Chiaraluce, L.: From surface geology to aftershock
 931 analysis: constraints on the geometry of the L'Aquila 2009 seismogenic fault system. *Italian J. Geosciences* 131 (3), 330-347,
 932 2012a.

933

934 Lavecchia, G., de Nardis, R., Cirillo, D., Brozzetti, F., and Boncio, P.: The May-June 2012 Ferrara Arc earthquakes (northern
 935 Italy): structural control of the spatial evolution of the seismic sequence and of the surface pattern of coseismic fractures,
 936 *Annals of Geophysics*, 55, 4, doi: 10.4401/ag-6173, 2012b

937

938 Lavecchia G., de Nardis, R., Costa, G., Tiberi, L., Ferrarini, F., Cirillo, D., Brozzetti F., and Suhadolc, P.: Was the Mirandola
 939 thrust really involved in the Emilia 2012 seismic sequence (northern Italy)? Implications on the likelihood of triggered
 940 seismicity effects, *Boll. Geof. Teor. Appl.*, Vol. 56, n. 4, pp. 461- 488, 2015.

941

942 Lavecchia, G., Castaldo, R., de Nardis, R., De Novellis, V., Ferrarini, F., Pepe, S., Brozzetti, F., Solaro, G., Cirillo, D., Bonano,
 943 M., Boncio, P., Casi, F., De Luca, C., Lanar, R., Manunta, M., Manzo, M., Pepe, A., Zinno, I., and Tizzani, P.: Ground
 944 deformation and source geometry of the 24 August 2016 Amatrice earthquake (Central Italy) investigated through analytical
 945 and numerical modeling of DInSAR measurements and structural-geological data, *Geophys. Res. Lett.*, 43,
 946 <https://doi.org/10.1002/2016GL071723>, 2016

947

948 Lavecchia, G., Adinolfi, G. M., de Nardis, R., Ferrarini, F., Cirillo, D., Brozzetti, F., De Matteis, R., Festa, G., and Zollo, A.:
 949 Multidisciplinary inferences on a newly recognized active east-dipping extensional system in central Italy, *Terra Nova*, 29,
 950 77-89, <https://doi.org/10.1111/ter.12251>, 2017.

951

952 Lavecchia, G., de Nardis, R., Ferrarini, F., Cirillo, D., Bello, S., and Brozzetti, F.: Regional seismotectonic zonation of
 953 hydrocarbon fields in active thrust belts: a case study from Italy, in *Building knowledge for geohazard assessment and*
 954 *management in the caucasus and other orogenic regions*, Editors F. L. Bonali, F. Pasquaré Mariotto, and N. Tsereteli (the
 955 Netherlands: Springer), doi:10.1007/978-94-024-2046-3, 2021.

956

957 Leonard, M.: Earthquake fault scaling: Relating rupture length, width, average displacement, and moment release, Bull.
958 Seismol. Soc. Am., 100(5A), 1971-1988. <https://doi.org/10.1785/0120090189>, 2010.

959

960 Liberi, F., Morten, L., and Piluso, E.: Geodynamic significance of the ophiolites within the Calabrian Arc, Island Arc, 15, 26–
961 43, <https://doi.org/10.1111/j.1440-1738.2006.00520.x>, 2006.

962

963 Liberi, F., and Piluso, E.: Tectonometamorphic evolution of the ophiolitic sequences from Northern Calabrian Arc, Italian
964 Journal Geoscience (Boll. Society Geological Italian), 128, 483–493, <https://doi.org/10.3301/IJG.2009.128.2.483>, 2009.

965

966 Lippmann-Provansal, M. : L'Appennin meridionale (Italie): Etude geomorphologique, these Doctorat, Univ. D'Aix-Marseille
967 II, Marseille, France, 1987.

968

969 Lomax, A., Virieux, J., Volant, P., and Berge-Thierry, C.: Probabilistic Earthquake Location in 3D and Layered Model, in
970 Advances in Seismic Event Location, Pp. 101-134, Kluwer Academic Publishers, Netherlands, 2000.

971

972 Margheriti, L., Amato, A., Braun, T., Cecere, G., D'Ambrosio, C., De Gori, and P., Selvaggi, G.: Emergenza nell'area del
973 Pollino: le attività della Rete Sismica Mobile, Rapporti Tecnici INGV, 2013.

974

975 Mariucci, M.T., and Montone, P.: Database of Italian present-day stress indicators, IPSI 1.4, Sci. Data 7, 298.
976 <https://doi.org/10.1038/s41597-020-00640-w>, 2020.

977

978 Maschio, L., Ferranti, L., and Burrato, P.: Active extension in Val d'Agri area, southern Apennines, Italy: Implications for the
979 geometry of the seismogenic belt, Geophys. J. Int., 162, 591–609, <https://doi.org/10.1111/j.1365-246X.2005.02597.x>, 2005.

980

981 Mattei, M., Cifelli, F., and , D'Agostino N.: The evolution of the Calabrian Arc: Evidence from paleomagnetic and GPS
982 observations, Earth and Planetary Science Letters, 263 (3-4), 259 – 274, 10.1016/j.epsl.2007.08.034, 2007.

983

984 Michetti, A. M., Ferrel, L., Serva, L., and Vittori, E.: Geological evidence for strong historical earthquakes in an "aseismic"
985 region: The Pollino case (Southern Italy), Journal of Geodynamics, 24:1-4, 67-86. [https://doi.org/10.1016/S0264-3707\(97\)00018-5](https://doi.org/10.1016/S0264-3707(97)00018-5), 1997.

986
987

988 Michetti, A. M., Ferreli, L., Esposito, E., Porfido, S., Blumetti, A. M., Vittori, E., Serva, L., and Roberts, G. P.: Ground Effects
 989 during the 9 September 1998, Mw = 5.6 Lauria, Earthquake and the Seismic Potential of the seismic Pollino Region in Southern
 990 Italy, *Seismological Research Letters*, 71(1), 31-46. <https://doi.org/10.1785/gssrl.71.1.31>, 2000.
 991
 992 Montone, P., and Mariucci, M.T.: The New Release of the Italian Contemporary Stress Map, *Geophys. J. Int.*, 205 (3), 1525–
 993 1531. <https://doi.org/10.1093/gji/ggw100>, 2016.
 994
 995 Mostardini, F., and Merlini, S.: Appennino centro meridionale - Sezioni geologiche e proposta di modello strutturale. *Mem.*
 996 *Soc. Geol. Ital.* 35, 177–202, 1986
 997
 998 Napolitano, F., De Siena, L., Gervasi, A., Guerra, I., Scarpa, R., and La Rocca, M.: Scattering and absorption imaging of a
 999 highly fractured fluid-filled seismogenetic volume in a region of slow deformation, *Geosci. Front.*, 11(3), 989-998.
 1000 <https://doi.org/10.1016/j.gsf.2019.09.014>, 2020.
 1001
 1002 Napolitano, F., Galluzzo, D., Gervasi, A., Scarpa, R., La Rocca, M.: Fault imaging at Mt Pollino (Italy) from relative location
 1003 of microearthquakes, *Geophysical Journal International*, 224(1), 637-648, <https://doi.org/10.1093/gji/ggaa407> , 2021.
 1004
 1005 Nicholson, G., Plesch, A., Sorlion, C. C., Shaw, J. H., and Hauksson, E.: TheSCEC 3D community fault model (CFM-v5): an
 1006 updated and expanded fault set of oblique crustal deformation and complex fault interaction for southern California, *Eos Trans.*
 1007 *Am. Geophys. Union* 95 (52). Abstract T31B-4584, 2014.
 1008
 1009 Nicholson, C., Plesch, A., Sorlien, C. C., Shaw, J. H., and Hauksson, E.: The SCEC community fault model version 5.0: an
 1010 updated and expanded 3D fault set for southern California, in 2015 pacific section AAPG joint meeting program (Oxnard,
 1011 CA), Vol. 77, September 12-16, 2015.
 1012
 1013 Ogniben, L.: Schema introduttivo alla geologia del confine calabro-lucano, *Mem. Soc. Geol. It.* 8, 453-763, 1969.
 1014
 1015 Ogniben, L.: Schema geologico della Calabria in base ai dati odierni, *Geologia Romana*, 12, 243–585, 1973.
 1016
 1017 Orecchio, B., Presti, D., Totaro, C., Guerra, I., and Neri, G.: Imaging the velocity structure of the Calabrian Arc region (south
 1018 Italy) through the integration of different seismological data, *Boll. Geofis. Teor. Appl.* 52, 625-638, 2011,
 1019 http://www3.ogs.trieste.it/bgta/pdf/bgta0023_ORECCHIO.pdf last access: 19 April 2021.
 1020

1021 Pantosti, D., and Valensise, G.: Faulting mechanism and complexity of the november 23, 1980, Campania-Lucania earthquake,
 1022 inferred from surface observation, *J. Geophys. Res* 95, 15319. doi:10.1029/jb095ib10p15319, 1990.
 1023
 1024 Pantosti, D., and Valensise, G.: Source geometry and long-term behavior of the 1980, Irpinia earthquake fault based on field
 1025 geologic observations. *Ann. Geofisc* 36, 41–49. <https://doi.org/10.4401/ag-4299>, 1993.
 1026
 1027 Papanikolaou, I. D., and Roberts, G. P.: Geometry, kinematics and deformation rates along the active normal fault system in
 1028 the southern Apennines: implications for fault growth, *J. Struct. Geol* 29, 166-188. <https://doi.org/10.1016/j.jsg.2006.07.009>,
 1029 2007.
 1030
 1031 Passarelli, L., Hainzl, S., Cesca, S., Meccaferri, F., Mucciarelli, M., Roessler, D., Corbi, F., Dahm, T., and Rivalta, E.: Aseismic
 1032 transient driving the swarm-like seismic sequence in the Pollino range, Southern Italy, *Geophys. J. Int.*, 201(3), 1553–1567,
 1033 <https://doi.org/10.1093/gji/ggv111>, 2015.
 1034
 1035 Pastori, M., Margheriti, L., De Gori, P., Govoni, A., Lucente, F.P., Moretti, M., Marchetti, A., Di Giovambattista, R., Anselmi,
 1036 M., De Luca, P., Nardi, A., Agostinetti, N.P., Latorre, D., Piccinini, D., Passarelli, L., and Chiarabba, C.: The 2011–2014
 1037 Pollino Seismic Swarm: Complex Fault Systems, Imaged by 1D Refined Location and Shear Wave Splitting Analysis at the
 1038 Apennines–Calabrian Arc Boundary, *Front. Earth Sci.* 9:618293. doi: 10.3389/feart.2021.618293, 2021.
 1039
 1040 Patacca, E., and Scandone, P.: Geological interpretation of the CROP-04 seismic line (Southern Apennines, Italy), *Boll. Soc.*
 1041 *Geol. It. (Ital. J. Geosci.)*, 7, 297-315, 2007.
 1042
 1043 Plesch, A., Shaw, J. H., and Jordan, T. H.: Stochastic descriptions of basin velocity structure from analyses of sonic logs and
 1044 the SCEC community velocity model (CVM-H), in Presentation at 2014 SSA annual meeting, Palm Springs, CA, September
 1045 6-10, 2014.
 1046
 1047 Pondrelli, S., Salimbeni, S., Ekström, G., and Morelli, A.: The Italian CMT dataset from 1977 to the present, *Phys. Earth*
 1048 *Planet. In* 159, 286–303, <https://doi.org/10.1016/j.pepi.2006.07.008>, 2006.
 1049
 1050 Porreca, M., Minelli, G., Ercoli, M., Brobia, A., Mancinelli, P., Cruciani, F., Giorgetti, C., Carboni, F., Mirabella, F., Cavinato,
 1051 G., Cannata, A., Pauselli, C., and Barchi, M. R.: Seismic reflection profiles and subsurface geology of the area interested by
 1052 the 2016–2017 earthquake sequence (Central Italy), in: The 2016 Central Italy Seismic Sequence: Insights, implications and
 1053 lessons learned, *Tectonics*, 37, 1116–1137, <https://doi.org/10.1002/2017TC004915>, 2018.
 1054

1055 Porreca, M., Fabbrizzi, A., Azzaro, S., Pucci, S., Del Rio, L., Pierantoni, P. P., Giorgetti, C., Roberts, G., and Barchi, M. R.:
 1056 3D geological reconstruction of the M. Vettore seismogenic fault system (Central Apennines, Italy): Cross-cutting relationship
 1057 with the M. Sibillini thrust, *J. Struct. Geol.*, 131, 103938, <https://doi.org/10.1016/j.jsg.2019.103938>, 2020.
 1058
 1059 Presti, D., Troise, C., and De Natale, G.: Probabilistic location of seismic sequences in heterogeneous media, *Bull. Seismol.*
 1060 *Soc. Am.* 94, 2239-2253, DOI: 10.1785/0120030160, 2004.
 1061
 1062 Presti, D., Orecchio, B., Falcone, G., and Neri, G.: Linear versus nonlinear earthquake location and seismogenic fault detection
 1063 in the southern Tyrrhenian Sea. Italy, *Geophys. J. Int.* 172, 607-618, <https://doi.org/10.1111/j.1365-246X.2007.03642.x>, 2008.
 1064
 1065 Robustelli, G., Russo Ermolli, E., Petrosino, P., Jicha, B., Sardella, R., and Donato, P.: Tectonic and climatic control on
 1066 geomorphological and sedimentary evolution of the Mercure basin, southern Apennines, Italy, *Geomorphology* 214, 423-435,
 1067 <https://doi.org/10.1016/j.geomorph.2014.02.026>, 2014.
 1068
 1069 Ross, Z. E., Cochran, E. S., Trugman, D. T., and Smith, J. D.: 3D Fault Architecture Controls the Dynamism of Earthquake
 1070 Swarms. *Science* 368, 1357–1361. Doi:10.1126/science.abb0779, 2020.
 1071
 1072 Rovida, A., Locati, M., Camassi, R., Lolli, B., and Gasperini, P.: The Italian earthquake catalogue CPTI15, *Bulletin of*
 1073 *Earthquake Engineering*, 18, 2953-2984, <https://doi.org/10.1007/s10518-020-00818-y>, 2020.
 1074
 1075 Rovida A., Locati M., Camassi R., Lolli B., Gasperini P., and Antonucci A.: Catalogo Parametrico dei Terremoti Italiani
 1076 (CPTI15), versione 3.0. Istituto Nazionale di Geofisica e Vulcanologia (INGV). <https://doi.org/10.13127/CPTI/CPTI15.3>,
 1077 2021.
 1078
 1079 Sato, H., Hirata, H., Ito, T., Tsumura, N., and Ikawa, T.: Seismic reflection profiling across the seismogenic fault of the 1995
 1080 Kobe earthquake, southwestern Japan, *Tectonophysics*, 286 (1–4), 19-30, [https://doi.org/10.1016/S0040-1951\(97\)00252-7](https://doi.org/10.1016/S0040-1951(97)00252-7),
 1081 1998.
 1082
 1083 SCEC, 2021 <https://www.scec.org/research/cfm>; last access: 19 April 2021.
 1084
 1085 Schiattarella, M., Torrente, M., and Russo, F.: Analisi strutturale ed osservazioni morfotettoniche nel bacino del Mercure
 1086 (Confine calabro-lucano), *Il Quaternario*, 7, 613-626, 1994.
 1087

1088 Scognamiglio, L., Tinti, E., and Quintiliani, M.: Time Domain Moment Tensor (TDMT) [Data set]. Istituto Nazionale di
 1089 Geofisica e Vulcanologia (INGV). <https://doi.org/10.13127/TDMT>, 2006.

1090

1091 Servizio Geologico d'Italia: 220 Verbicaro sheet of the Carta Geologica D'Italia, 1. 100.000 Scale. Rome, 1970.

1092

1093 Sgambato, C., Walker, J. P. F., and Roberts, G. P.: Uncertainty in strain-rate from field measurements of the geometry, rates
 1094 and kinematics of active normal faults: implications for seismic hazard assessment, *J. Struct. Geol.* 131,
 1095 103934.doi:10.1016/j.jsg.2019.103934, 2020.

1096

1097 Sketsiou, P., De Siena, L., Gabrielli, S., and Napolitano, F.: 3-D attenuation image of fluid storage and tectonic interactions
 1098 across the Pollino fault network, *Geophysical Journal International*, 226(1), 536–547, <https://doi.org/10.1093/gji/ggab109>,
 1099 2021.

1100

1101 Sperner, B., Müller, B., Heidbach, O., Delvaux, D., Reinecker, J., and Fuchs, K.: Tectonic stress in the Earth's crust: advances
 1102 in the World Stress Map project. In: *New Insights into Structural Interpretation and Modelling* (D.A. Nieuwland, ed.), *J. Geol.*
 1103 *Soc. London Spec. Publ.*, 212, 101–116, <https://doi.org/10.1144/GSL.SP.2003.212.01.07>, 2003.

1104

1105 Spina, V., Galli, P., Tondi, E., and Mazzoli, S.: Fault propagation in a seismic gap area (northern Calabria, Italy): implications
 1106 for seismic hazard, *Tectonophysics*, 476, 357-369, <https://doi.org/10.1016/j.tecto.2009.02.001>, 2009.

1107

1108 Stirling, M., Goded, T., Berryman, K. and Litchfield, N.: Selection of Earthquake Scaling Relationships for Seismic-Hazard
 1109 Analysis, *Bulletin of the Seismological Society of America*, 103(6), 2993-3011. <https://doi.org/10.1785/0120130052>, 2013.

1110

1111 Tangari, A.C., Scarciglia, F., Piluso, E., Marinangeli, L., and Pompilio, L.: Role of weathering of pillow basalt, pyroclastic
 1112 input and geomorphic processes on the genesis of the Monte Cerviero upland soils (Calabria, Italy), *Catena*, 171, 299-315,
 1113 ISSN 0341-8162, <https://doi.org/10.1016/j.catena.2018.07.015>, 2018.

1114

1115 Tarquini, S., Vinci, S., Favalli, M., Doumaz, F., Fornaciai, A., and Nannipieri, L.: Release of a 10-m-resolution DEM for the
 1116 Italian territory: Comparison with global-coverage DEMs and anaglyph-mode exploration via the web, *Computers and*
 1117 *Geosciences*, 38, 168-170. <https://doi.org/10.1016/j.cageo.2011.04.018>, 2012.

1118

1119 TDMT database – INGV <http://cnt.rm.ingv.it/tdmt>. last access: 19 April 2021.

1120

1121 Tertulliani, A., and Cucci, L.: New insights on the strongest historical earthquake in the Pollino region (southern Italy),
 1122 Seismol. Res. Lett., 85(3), 743-751, <https://doi.org/10.1785/0220130217>, 2014.
 1123
 1124 Totaro, C., Presti, D., Billi, A., Gervasi, A., Orecchio, B., Guerra, I., and Neri, G.: The ongoing seismic sequence at the Pollino
 1125 Mountains, Italy. Seismol. Res. Let., 84(6), 955-962, <https://doi.org/10.1785/0220120194>, 2013.
 1126
 1127 Totaro, C., Koulakov, I., Orecchio, B., and Presti, D.: Detailed crustal structure in the area of the southern Apennines–Calabrian
 1128 Arc border from local earthquake tomography, J. Geodyn., 82, 87-97, <https://doi.org/10.1016/j.jog.2014.07.004>, 2014.
 1129
 1130 Totaro, C., Seeber, L., Waldhauser, F., Steckler, M., Gervasi, A., Guerra, I., Orecchio, B., and Presti, D.: An intense earthquake
 1131 swarm in the southernmost Apennines: fault architecture from high-resolution hypocenters and focal mechanisms, Bull.
 1132 Seismol. Soc. Am. 105, 1-6. <https://doi.org/10.1785/0120150074>, 2015.
 1133
 1134 Totaro, C., Orecchio, B., Presti, D., Scolaro, S., and Neri G.: Seismogenic stress field estimation in the Calabrian Arc region
 1135 (south Italy) from a Bayesian approach, Geophys. Res. Lett., 43, 8960–8969, <https://doi.org/10.1002/2016GL070107>, 2016.
 1136
 1137 Valoroso, L., Chiaraluce, L., Di Stefano, R., and Monachesi, G.: Mixed-Mode Slip Behavior of the Altotiberina Low-Angle
 1138 Normal Fault System (Northern Apennines, Italy) through High-Resolution Earthquake Locations and Repeating Events, J.
 1139 Geoph. Res. Solid Earth, 122(12), 10220-10240, <https://doi.org/10.1002/2017JB014607>, 2017.
 1140
 1141 Van Dijk, J.P., Bello, M., Brancaloni, G.P., Cantarella, G., Costa, V., Frixia, A., Golfetto, F., Merlini, S., Riva, M., Toricelli,
 1142 S., Toscano, C., and Zerilli, A.: A regional structural model for the northern sector of the Calabrian Arc (southern Italy),
 1143 Tectonophysics 324, 267-320, [https://doi.org/10.1016/S0040-1951\(00\)00139-6](https://doi.org/10.1016/S0040-1951(00)00139-6), 2000.
 1144
 1145 Vezzani, L., Festa, A., and Ghisetti, F.C.: Geology and tectonic evolution of the Central-Southern Apennines, Italy, Special
 1146 Paper of the Geological Society of America, 469, 1-58, <https://doi.org/10.1130/SPE469>, 2010.
 1147
 1148 Villani, F., and Pierdominici, S.: Late Quaternary tectonics of the Vallo di Diano basin (southern Apennines, Italy), Quat. Sci.
 1149 Rev., 29, 3167-3183. <https://doi.org/10.1016/j.quascirev.2010.07.003>, 2010
 1150
 1151 Waldhauser F., and Ellsworth W.: A Double-Difference Earthquake Location Algorithm: Method and Application to the
 1152 Northern Hayward Fault, California, Bull. Seism. Soc. Am. 90(6):1353-1368, <http://dx.doi.org/10.1785/0120000006>, 2000.
 1153

1154 Waldhauser, F.: HypoDD: a Computer Program to Compute Double Difference Earthquake Locations. U.S. Geol. Surv, Menlo
 1155 Park, California, pp. 01-113. Open-File Report, 2001.
 1156
 1157 Wells, D.L., and Coppersmith, K.J.: New empirical relationships among magnitude, rupture length, rupture width, rupture
 1158 area, and surface displacement, Bull. Seismol. Soc. Am., 84(4), 974-1002, 1994.
 1159
 1160 Wesnousky, S.G.: Displacement and geometrical characteristics of earthquake surface ruptures: Issues and implications for
 1161 seismic hazard analysis and the process of earthquake rupture, Bull. Seismol. Soc. Am., 98(4), 1609-1632.
 1162 <https://doi.org/10.1785/0120070111>, 2008.
 1163
 1164 Westoby, M.J., Brasington, J., Glasser, N.F., Hambrey, M.J., and Reynolds, J.M.: ‘Structure-from-motion’ photogrammetry:
 1165 A low-cost, effective tool for geoscience applications, Geomorphology, 179, 300–314, 2012.